INTERNATIONAL JOURNAL OF ROBUST AND NONLINEAR CONTROL
Int. J. Robust. Nonlinear Control (2012)
Published online in Wiley Online Library (wileyonlinelibrary.com). DOI: 10.1002/rnc.2872

Stability and robustness of large platoons of vehicles with double-integrator models and nearest neighbor interaction

He Hao*,† and Prabir Barooah

Department of Mechanical and Aerospace Engineering, University of Florida, Gainesville, FL 32611, USA

SUMMARY

We study the stability and robustness of a large platoon of vehicles, where each vehicle is modeled as a double integrator, for two decentralized control architectures: predecessor following and symmetric bidirectional. In the predecessor-following architecture, the control action on each agent only depends on the information from its immediate front neighbor, whereas in the symmetric bidirectional architecture, it depends equally on the information from both its immediate front neighbor and back neighbor. We prove asymptotic stability of the formation for a class of nonlinear controllers with sector nonlinearity, with the linear controller as a special case. We show that the convergence rate of the predecessor-following architecture is much faster than that of the symmetric bidirectional architecture. However, the predecessor-following architecture suffers high algebraic growth of initial errors. We also establish scaling laws (with N) of certain H_∞ norms of the formation that measure its robustness to external disturbances for the linear case. It is shown that the robustness performance grows geometrically in N for predecessor-following architecture but only polynomially in N for symmetric-bidirectional architecture. Extensive numerical simulations are conducted to verify the predictions for the linear case and empirically estimate the corresponding performance metrics for a saturation-type nonlinear controller. On the basis of the analytical and numerical results, it is seen that the symmetric bidirectional architecture outperforms the predecessor-following architecture in all measures of performance. Within the predecessor-following architecture, the nonlinear controller is seen to perform better in general than the linear one. A number of design guidelines are provided on the basis of these conclusions. Copyright © 2012 John Wiley & Sons, Ltd.

Received 15 August 2011; Revised 31 May 2012; Accepted 23 June 2012

KEY WORDS: multi-agent systems; convergence rate; H_∞ norm; nonlinear control; distributed control

1. INTRODUCTION

Cooperative control of multi-agent systems has spurred an extensive interest in the control community because of its wide range of applications such as in automated highway system [1, 2]; coordination of aerial, ground, and autonomous vehicles for surveillance and rescue [3]; spacecraft formation control for science missions [4]; and in collective behavior of bird flocks and animal swarms [5]. Among these applications, one of the most well-studied problems is autonomous intelligent cruise control of large vehicular platoons (see [6–9] and references therein). The primary goal of autonomous intelligent cruise control is to increase traffic throughput and safety.

One of the most important problems in autonomous intelligent cruise control of platoons is string instability or slinky-type effect [10–12]. To solve this problem, different control policies and control architectures are considered. In [11], a constant headway control law is developed to insure string stability. However, the constant headway policy by itself is not enough; the headway has to be *large enough* to avoid the problems associated with constant spacing policy [13]. Because one of the main

*Correspondence to: He Hao, Department of Mechanical and Aerospace Engineering, University of Florida, Gainesville, FL 32611, USA.
†E-mail: hehao@ufl.edu

Copyright © 2012 John Wiley & Sons, Ltd.

motivations for automated platooning is to achieve higher highway capacity by making cars move with a small inter-vehicle separation, there is a need to study the constant spacing policy. It was shown in [11, 14, 15] that, with constant spacing policy, the leader's information need to be broadcasted to the following vehicles to assure string stability. Nevertheless, the inevitable time delay and package drop in broadcasting the leader's information will cause string instability [16]. This leads to the study of decentralized control architecture, that is, each vehicle can only use measurements of relative position and/or velocity with respect to its nearest neighbors.

Two decentralized control architectures that are commonly examined are predecessor-following and bidirectional architectures. In the *predecessor-following* architecture, the control action on each vehicle only depends on the relative information from its immediate predecessor, that is, the vehicle in front of it. In the bidirectional architecture, the control depends on the relative information from both its immediate predecessor and follower. Within the bidirectional architecture, the most commonly analyzed case is the *symmetric bidirectional* architecture, in which the control at a vehicle depends on the information from both of its neighbors *equally*.

A typical issue in distributed/decentralized control is that, as the number of agents in the system increases, the performance of the closed-loop degrades progressively. It has been established that the predecessor-following architecture suffers from high sensitivity to external disturbances with linear control [17, 18]. High sensitivity to external disturbance is typically referred to as slinky-type effect [19, 20] or string instability [21]. Seiler *et al.* showed that, with linear control, the poor robustness performance with the predecessor-following architecture is independent of the design of the controller but a fundamental artifact of the architecture [14]. The robustness performance can be improved by nonidentical linear controllers but at the expense of the control gains increasing without bound as the number of the vehicles increases [11, 22]. It was shown in [14, 15, 21, 23] that the symmetric bidirectional architecture also suffers from poor sensitivity to external disturbances.

Although a rich literature exists on sensitivity to disturbances for predecessor-following and symmetric bidirectional architectures with linear control, to the best of our knowledge, a precise comparison of these two architectures is lacking. Moreover, most of the works on formation control have been limited to linear control laws, whereas little is known about nonlinear control. Nonlinear terms in the closed-loop dynamics may arise from either purposefully designed nonlinear control laws (if beneficial) or unavoidable nonlinearities in the agent dynamics, such as actuator saturation. Both of these cases can be analyzed by considering linear plant dynamics and nonlinear controllers.

In this paper, we examine the stability and robustness (sensitivity to external disturbances) of a large platoon of vehicles with linear as well as a class of nonlinear controllers, for both predecessor-following and symmetric bidirectional architectures. Each vehicle is modeled as a fully actuated point mass (double integrator). A few authors have used first-order kinematic models by ignoring vehicle inertia. However, in general, kinematic models (single integrator) fail to reproduce the slinky-type effects that are exhibited by kinetic models (double integrator).

We prove stability of the closed loop with an arbitrary number of agents for a class of nonlinear controllers where the control gain functions satisfy certain sector conditions. The difference between the transient responses of the two architectures in case of linear control is explained by the expressions we derive for the least stable eigenvalue of the closed-loop state matrix and its multiplicity. In particular, we show that the predecessor-following architecture has a larger convergence rate compared with the symmetric bidirectional architecture: $O(1)$ versus $O(1/N^2)$. It is worthwhile to mention that the convergence rate of the formation with symmetric bidirectional architecture scales poorly as a function of N even with centralized linear quadratic regulator control [24]. The real part of the least stable eigenvalue with linear quadratic regulator control scales as $O(1/N)$. However, the predecessor-following architecture suffers from algebraic growth of initial conditions because of the high multiplicity of the least stable eigenvalue. For the nonlinear control, we study the transient performance through numerical simulations. The simulations show that, in the predecessor-following architecture, the transient response is significantly improved by using a saturation-type nonlinearity in the control gain instead of a linear control.

Next, we examine the closed loop's performance in terms of the sensitivity to external disturbances. Specifically, we examine the *first-to-last amplification factor*, defined as the L_2 gain from a disturbance injected at the first vehicle to the position tracking error of the last vehicle, and *all-to-all*

Copyright © 2012 John Wiley & Sons, Ltd.

DOI: 10.1002/rnc

amplification factor, which is defined as the L_2 gain from the disturbances acting on all the vehicles to their position tracking errors. In case of linear controllers, we show that, when N is large, the first-to-last amplification factor, which becomes an H_∞ norm, grows as $O(\alpha^N)$, $\alpha > 1$, for predecessor-following architecture but only as $O(N)$ for the symmetric bidirectional architecture. The all-to-all amplification factor scales as $O(\alpha^N)$ for predecessor-following architecture and as $O(N^3)$ for the symmetric bidirectional architecture. The first result is known in the literature [14]. These results establish a precise comparison between the robustness of symmetric bidirectional and predecessor-following architectures with linear control. Namely, symmetric bidirectional architecture has a much smaller sensitivity to external disturbances.

Establishing scaling laws for robustness metrics with nonlinear controllers is challenging. We therefore study the response in the nonlinear case through extensive numerical simulations, with both sinusoidal and random disturbances as inputs, and estimate performance metrics from simulation data. We observe from these studies that, within the predecessor-following architecture, a nonlinear controller with a saturation-type nonlinearity performs better than the corresponding linear one. In the symmetric bidirectional architecture, the difference between the linear and nonlinear controller's performance is not significant.

The theoretical as well as numerical simulations lead to certain design guidelines. Comparing all four combinations (linear, nonlinear, predecessor following, and symmetric bidirectional), we observe that, for the same number of agents, the symmetric bidirectional architecture performs considerably better (both in terms of transient decay and robustness to disturbances) than the predecessor-following one, and this conclusion is valid for both the linear and nonlinear control laws. Thus, the added complexity and cost of the symmetric bidirectional architecture due to additional sensors is justified. If stringent cost considerations allow only the predecessor-following architecture, then the nonlinear controller should be used over the linear one. Even with a linear control law, actuator saturation will make the overall system closer to the closed-loop nonlinear system studied. Therefore, the fact that both the linear and nonlinear controllers with sector nonlinearities are seen to perform comparably in the symmetric bidirectional architecture can be seen as a 'robustness to modeling errors' of this architecture. Some of the results for the linear predecessor-following case may be known or easily derived from existing results. We nevertheless include them for the sake of completeness.

The conclusions about the architectures are derived only for the specific control laws we investigated. The local control laws at the vehicles are either of proportional–derivative (PD) type (in the linear case) or such that their linearization around the origin are of PD type (in the nonlinear case). Nevertheless, analysis carried out with this controller structure and double-integrator vehicle models is relevant even if there are additional dynamic elements in the loop (i.e, either in the controller or in the vehicle dynamic model), at least in the linear case. Reasons for this can be seen from the results in [23], which considered vehicle models with two integrators in series with an additional transfer function (to model powertrain dynamics) and arbitrary LTI compensators. First, a dynamic controller cannot have a zero at the origin because it will result in a pole-zero cancellation causing the steady-state errors to grow without bound as N increases [23]. Second, a dynamic controller cannot have an integrator either if the vehicle model has two integrators. For if it does, the closed-loop platoon dynamics become unstable for sufficiently large values of N [23]. As a result, any allowable dynamic element in the loop must essentially act as a static gain at low frequencies. The results of [23] indicate that the principal challenge in controlling a platoon of vehicles arises because of the presence of a double integrator with its unbounded gain at low frequencies. Hence, the issues discussed here with a PD controller structure is also relevant to the case where additional dynamic elements appear in the loop.

In terms of the stability analysis with nonlinear controllers, our work closely parallels that of [25], which considers arbitrary information graphs (instead of the 1-D graph of a platoon we consider). However, the results of [25] are not applicable to the scenario considered here, because we consider relative velocity feedback, whereas [25] considers absolute velocity feedback. Furthermore, the assumption of symmetry made in [25] precludes the predecessor-following architecture from their formulation. In terms of sensitivity to external disturbances with linear control, our work is related to [26–30]. In [26, 27], it is shown that, if the information graph used is undirected and has

Copyright © 2012 John Wiley & Sons, Ltd.

DOI: 10.1002/rnc

bounded degree, the maximum error due to sinusoidal disturbances cannot be made independent of the size of the formation. In [28], Veerman showed that the first-to-last amplification grows linearly in N for the symmetric bidirectional case but grows exponentially in N for *asymmetric* bidirectional architecture, where asymmetric means the information from its front and back neighbors are weighted differently. Scaling laws of certain H_2 norms from disturbance to outputs that quantify a number of performance measures are examined in [29, 30]. In particular, it was shown that the 'all-to-all' H_2 norm scales exponentially in N for predecessor-following architecture (although with absolute velocity feedback) [30] but as $O(N^3)$ for the symmetric bidirectional architecture [29], which is the same as that of the all-to-all H_∞ norm established in this paper. They also show that the scaling laws for the H_2 norm hold for arbitrary but fixed number of front and back neighbors and arbitrary stabilizing feedback gains.

The rest of this paper is organized as follows. Section 2 presents the problem statement. Sections 3 and 4 present the stability and robustness analysis, respectively, along with corresponding numerical studies. The paper ends with a summary in Section 5.

2. PROBLEM STATEMENT

We consider the formation control of N homogeneous agents that are moving in 1-D Euclidean space, as shown in Figure 1. The position of the ith agent is denoted by p_i, and each agent is modeled as a double integrator:

$$\ddot{p}_i = u_i + w_i, \quad i \in \{1, 2, \cdots, N\}, \tag{1}$$

where u_i is the control input and w_i is the external disturbance. This is a commonly used model for vehicle dynamics in studying vehicular platoons and results from feedback linearization of nonlinear vehicle dynamics [11, 31].

The control objective is to make the network of agents maintain a rigid formation geometry while following a desired trajectory. The desired geometry of the formation is specified by the *desired gaps* $\Delta_{(i-1,i)}$ for $i \in \{1, \cdots, N\}$, where $\Delta_{(i-1,i)}$ is the desired value of $p_{i-1}(t) - p_i(t)$. The desired inter-vehicular gaps $\Delta_{(i-1,i)}$ are positive constants, and they have to be specified in a mutually consistent fashion, $\Delta_{(i,k)} = \Delta_{(i,j)} + \Delta_{(j,k)}$ for every triple (i, j, k), where $i \leqslant j \leqslant k$. The desired trajectory of the formation is provided in terms of a *fictitious* reference agent with index 0, whose trajectory is denoted by $p_0^*(t)$. The information on the desired trajectory of the formation is only provided to agent 1. The desired trajectory of the ith agent, $p_i^*(t)$, is given by

$$p_i^*(t) = p_0^*(t) - \Delta_{(0,i)} = p_0^*(t) - \sum_{j=1}^{i} \Delta_{(j-1,j)}. \tag{2}$$

In this paper, we consider the following two *decentralized* control architectures:

(i) *Predecessor-following architecture*. The control action at the ith agent depends on the relative position and velocity measurements from its immediate front neighbor. In particular, we consider the following decentralized control law:

$$u_i = -f(p_i - p_{i-1} + \Delta_{(i-1,i)}) - g(\dot{p}_i - \dot{p}_{i-1}), \tag{3}$$

where $i \in \{1, 2, \cdots, N\}$ and $f, g : \mathbb{R} \to \mathbb{R}$ are scalar functions.

Figure 1. Desired geometry of a 1-D network of N double-integrator agents. The reference agent with index '0' need not to be a real agent; it merely provides the reference trajectory of the formation to agent 1.

Copyright © 2012 John Wiley & Sons, Ltd.

DOI: 10.1002/rnc

(ii) *Symmetric bidirectional architecture*. The control action at the ith agent depends on the relative position and velocity measurements from its immediate front and back neighbors, and the information from its front and back neighbors are weighted equally. In particular, we consider the following decentralized control law:

$$\begin{aligned} u_i &= -f(p_i - p_{i-1} + \Delta_{(i-1,i)}) - g(\dot{p}_i - \dot{p}_{i-1}) \\ &\quad - f(p_i - p_{i+1} - \Delta_{(i,i+1)}) - g(\dot{p}_i - \dot{p}_{i+1}), \\ u_N &= -f(p_N - p_{N-1} + \Delta_{(N-1,N)}) - g(\dot{p}_N - \dot{p}_{N-1}), \end{aligned} \tag{4}$$

where $i \in \{1, 2, \cdots, N-1\}$ and $f, g : \mathbb{R} \to \mathbb{R}$.

In both architectures, the information needed to compute the control action at each agent can be easily obtained by on-board sensors such as radars, because only relative position and velocity are used in the control.

In this paper, we make the following assumptions.

Assumption 1

In the aforementioned controllers (3) and (4), the possibly nonlinear functions $f, g : \mathbb{R} \to \mathbb{R}$ are odd functions, which are smooth enough to guarantee the existence of a solution of the coupled ODEs. Each agent i knows the desired gaps $\Delta_{(i-1,i)}$ and $\Delta_{(i,i+1)}$, whereas only agent 1 knows the desired trajectory $p_0^*(t)$ of the fictitious reference agent. The reference trajectory is a constant velocity type, that is, $p_0^*(t) = v_0 t + c_0$ for some constants v_0 and c_0. The first agent must have access to its own absolute position and velocity information.

To facilitate analysis, we define the following position tracking error:

$$\tilde{p}_i := p_i - p_i^*, \tag{5}$$

where p_i^* is given by (2). The closed-loop dynamics for the predecessor-following architecture can now be expressed as the following coupled-ODE model:

$$\ddot{\tilde{p}}_i = -f(\tilde{p}_i - \tilde{p}_{i-1}) - g\left(\dot{\tilde{p}}_i - \dot{\tilde{p}}_{i-1}\right) + w_i, \quad i \in \{1, 2, \cdots, N\}. \tag{6}$$

The closed-loop dynamics for the symmetric bidirectional architecture are

$$\begin{aligned} \ddot{\tilde{p}}_i &= -f(\tilde{p}_i - \tilde{p}_{i-1}) - g\left(\dot{\tilde{p}}_i - \dot{\tilde{p}}_{i-1}\right) - f(\tilde{p}_i - \tilde{p}_{i+1}) - g\left(\dot{\tilde{p}}_i - \dot{\tilde{p}}_{i+1}\right) + w_i, \quad i < N, \\ \ddot{\tilde{p}}_N &= -f(\tilde{p}_N - \tilde{p}_{N-1}) - g\left(\dot{\tilde{p}}_N - \dot{\tilde{p}}_{N-1}\right) + w_N. \end{aligned} \tag{7}$$

Note that $\tilde{p}_0(t) = \dot{\tilde{p}}_0(t) \equiv 0$, because the reference agent perfectly tracks its desired trajectory. The system can be expressed in the state space form,

$$\dot{x} = \mathbf{f}(x, w), \tag{8}$$

where the state and disturbance vectors are defined as $x := [\tilde{p}_1, \dot{\tilde{p}}_1, \cdots, \tilde{p}_N, \dot{\tilde{p}}_N]^{\mathrm{T}}$ and $w := [w_1, \cdots, w_N]^{\mathrm{T}}$. The special case $f(z) = k_0 z$ and $g(z) = b_0 z$ (where z is the argument, $k_0 > 0$, and $b_0 > 0$) in the aforementioned coupled ODEs correspond to the case of *linear control* in each architecture. In the case of linear control, the closed-loop can be represented as

$$\dot{x} = Ax + Bw, \tag{9}$$

where A is the state matrix that depends on k_0 and b_0, and B is the input matrix with appropriate dimension.

In this paper, we study the stability of the origin $x = 0$ of the undisturbed system $\dot{x} = \mathbf{f}(x, 0)$ given in (8) with linear as well as a class of nonlinear controllers for the two architectures. In addition, we examine the sensitivity of position tracking errors $\tilde{p} = [\tilde{p}_1, \cdots, \tilde{p}_N]^{\mathrm{T}}$ to the external disturbances $w = [w_1, \cdots, w_N]^{\mathrm{T}}$.

Copyright © 2012 John Wiley & Sons, Ltd.

DOI: 10.1002/rnc

3. STABILITY ANALYSIS

In this section, we present the stability analysis of the origin $x = 0$ of the undisturbed system $\dot{x} = \mathbf{f}(x, 0)$ given in (8) with both linear and nonlinear controllers. For the linear case, we also derive formulae showing how the least stable eigenvalue of the state matrix A in (9) changes with increasing size of the formation. This eigenvalue quantifies the system's convergence rate with respect to initial errors. For the case of nonlinear controller, we provide sufficient conditions for asymptotic stability. Because convergence rates for nonlinear systems are difficult to obtain analytically, we perform numerical simulations to study the convergence rate with nonlinear controllers and compare with corresponding linear controllers. All simulations for studying transient performance correspond to the following scenario: the disturbance acting on each agent is zero; we perturb the initial position of the first agent from its desired value and observe the position tracking error of the last agent $\tilde{p}_N(t)$. For the convenience of comparison, we define the following as a measure of transient performance:

$$E := \lim_{T\to\infty} \frac{1}{x_0^2} \int_0^T \frac{1}{2} k_0 \tilde{p}_N^2(t) + \frac{1}{2} \dot{\tilde{p}}_N^2(t)\, \mathrm{d}t, \tag{10}$$

where $k_0 > 0$ is the linear position gain given as before and x_0 is the initial error of the first agent:

$$\tilde{p}_1(0) = x_0. \tag{11}$$

The quantity E is called the *integral of transient energy*. We assume the limit in (10) exists, that is, the last agent has finite $\mathcal{L}_2$ energy. In numerical simulations, we use the following estimate of E:

$$\hat{E} := \frac{1}{x_0^2} \int_0^T \frac{1}{2} k_0 \tilde{p}_N^2(t) + \frac{1}{2} \dot{\tilde{p}}_N^2(t)\, \mathrm{d}t, \tag{12}$$

where T is sufficiently large such that all the errors die out. We study through numerical simulations how E scales with the number of agents N and the initial error x_0.

3.1. Stability analysis with linear control

In the statement of the next theorem, the *least stable eigenvalue* of a matrix refers to the eigenvalue with the largest real part.

Theorem 1
Consider a 1-D network of N double-integrator agents with linear control law, that is, $f(z) = k_0 z$ and $g(z) = b_0 z$. If $k_0 > 0$ and $b_0 > 0$, the closed-loop dynamics are exponentially stable for both the predecessor-following and symmetric bidirectional architectures. Under the same conditions, the following statements hold.

(i) With predecessor-following architecture, the least stable eigenvalue of the closed-loop state matrix A is $\mu_1 = \frac{-b_0+\sqrt{b_0^2-4k_0}}{2}$, and this eigenvalue occurs with multiplicity N.
(ii) With symmetric bidirectional architecture, when N is large, the least stable eigenvalue is given by $\mu_1 = -\frac{\pi^2 b_0}{8N^2} + \Im$, with multiplicity of 1, where $\Im$ is an imaginary number.

The first statement of the theorem seems to be well known in the community, although we were unable to find a reference for it. The proof of Theorem 1 is given in the Appendix.

Although stability guarantees that transients due to initial conditions decay to 0 as $t \to \infty$, the speed at which the transients decay depends quite strongly on the architecture and the controller design. For a linear system, an appropriate measure of this convergence rate is the absolute value of the real part of the least stable eigenvalue of state matrix A, as long as the least stable eigenvalue is not repeated. If the least stable eigenvalue is repeated, then algebraic growth (peaking) occurs. In that case, the convergence rate is proportional to $t^k \mathrm{e}^{\mathrm{Re}(\mu_1)t}$, where k is the algebraic multiplicity of the least stable eigenvalue μ_1. It follows from Theorem 1 that the real part of the least stable

Copyright © 2012 John Wiley & Sons, Ltd.

DOI: 10.1002/rnc

eigenvalue $\mathrm{Re}(\mu_1)$ in predecessor-following architecture is independent of N, whereas it decays to 0 with increasing N in symmetric bidirectional architecture. This makes the predecessor-following architecture appear to have faster convergence rate than the symmetric bidirectional architecture, especially for large N. However, the large algebraic multiplicity of the least stable eigenvalue in the predecessor-following architecture will cause large algebraic growth of the initial conditions before they decay to 0. Corroboration through numerical simulations is provided in Section 3.3.

3.2. Stability analysis with nonlinear control

The next two theorems are on the stability of the network with nonlinear controllers; their proofs are given in the Appendix. In the statements of the theorems that follow, we say that a scalar function f belongs to the sector $[\varepsilon, K]$ if $\varepsilon z^2 \leqslant z f(z) \leqslant K z^2, \forall\ z \in \mathbb{R}$, and it belongs to the sector $(0, \infty]$ if $z f(z) > 0,\ \forall\ z \neq 0$.

Theorem 2
Consider a 1-D network of double-integrator agents with predecessor-following architecture with controller (3). If $f, g : \mathbb{R} \to \mathbb{R}$ satisfy the sector conditions $f \in [\varepsilon_1, K_1]$ and $g \in [\varepsilon_2, K_2]$, where $0 < \varepsilon_1 \leqslant K_1 < \infty$ and $0 < \varepsilon_2 \leqslant K_2 < \infty$, then the origin $x = 0$ of the undisturbed dynamics $\dot{x} = \mathbf{f}(x, 0)$ (8) is globally asymptotically stable (GAS).

Theorem 3
Consider a 1-D network of double-integrator agents with symmetric bidirectional architecture with controller (4). If $f, g : \mathbb{R} \to \mathbb{R}$ satisfy the sector conditions $f \in (0, \infty]$ and $g \in (0, \infty]$, then the origin $x = 0$ of the undisturbed dynamics $\dot{x} = \mathbf{f}(x, 0)$ (8) is GAS.

Remark 1
Note that stability with the linear controllers are special cases of Theorems 2 and 3. Comparing the aforementioned two theorems, we notice that the requirement on the sector condition in the predecessor-following architecture is stricter than that in the symmetric bidirectional architecture. However, these sector conditions are only sufficient.

3.3. Numerical comparison between linear and nonlinear controllers for transient decay

Because every practical actuator has saturation limits, saturation-type nonlinearity is of particular interest. The saturation-type nonlinearity in controlling large platoon is practically important and draws many researchers' attention [32, 33]. Throughout this section, we consider the following specific linear and saturation-type nonlinear controllers. The control gain functions $f(z)$ and $g(z)$ used in controllers (3) and (4) are given by

$$\begin{aligned} \text{Linear: } & f(z) = k_0 z, && g(z) = b_0 z, \\ \text{Nonlinear: } & f(z) = B_1 \tanh(\gamma_1 z), && g(z) = B_2 \tanh(\gamma_2 z), \end{aligned} \tag{13}$$

where $k_0 = 1$, $b_0 = 0.5$, $B_1 = 5$, $\gamma_1 = 0.2$, $B_2 = 5$, and $\gamma_2 = 0.1$. The parameters have been chosen in such a way that the slopes of $f(z)$ and $g(z)$ near the origin are equal to k_0 and b_0, respectively. This is done to make the linear and nonlinear cases comparable to some extent. Note that these $f(z)$ and $g(z)$ do not satisfy the sector conditions assumed in Theorem 2 *globally* but only satisfy the sector conditions *locally*. However, the region in which they satisfy the sector condition can be made arbitrarily large by choosing sufficiently small ε_1 and ε_2.

We compare the convergence rate and transient performance between linear and nonlinear controllers through numerical simulations. Figure 2(a) depicts the transients of the 1-D network with linear and nonlinear controllers for predecessor-following architecture. The algebraic growth for linear controller that is predicted by Theorem 1 is observed. We also see that the nonlinear controller has a much smaller peak error than the linear controller. The transients in the symmetric bidirectional architecture are shown in Figure 2(b). We see that (i) the performance of the nonlinear case is similar to that of the linear controller and (ii) the peak value of the error is much smaller compared with that in the predecessor-following architecture, no matter if the controller is linear or nonlinear.

Copyright © 2012 John Wiley & Sons, Ltd.

DOI: 10.1002/rnc

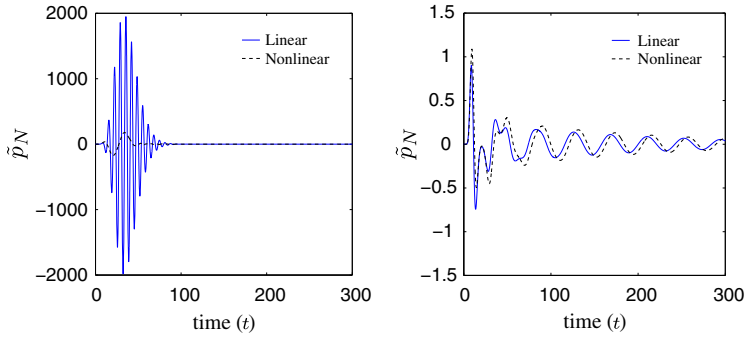

(a) Predecessor-following (b) Symmetric bidirectional

Figure 2. Comparison of transients of the position tracking error of the last agent for a network of $N = 10$ agents between linear and nonlinear controllers. The initial condition of the first agent used is $x_0 = 10$.

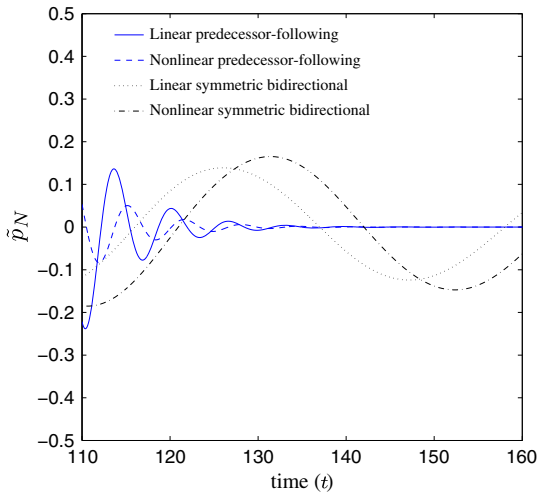

Figure 3. Comparison of convergence rate for a network of $N = 10$ agents between predecessor-following and symmetric bidirectional architectures. The initial condition of the first agent used is $x_0 = 10$.

Figure 3 shows a 'zoomed-in' version of the transient response. We see from the figure that the convergence rates of the linear and nonlinear controllers in each architecture are similar. In addition, the error in the predecessor-following architecture is smaller than in the case of symmetric bidirectional architecture for *large* t. This can be explained in the linear case from the real part of the least stable eigenvalue: it is much larger in the predecessor-following architecture compared with in the symmetric bidirectional architecture, $O(1)$ versus $O(1/N^2)$ (recall Theorem 1). The similarity between the simulation results in the nonlinear and linear cases indicates that the convergence rate in the predecessor-following architecture is higher than that in the symmetric bidirectional one, whether control is linear or nonlinear.

Figures 4 and 5 show the estimate of energy measure $\hat{E}$ for $T = 10^4$ s (defined in (12)) as a function of N and x_0, respectively. Recall that x_0 is the initial position error of the first agent; it is given in (11). We see that (i) the energy in the predecessor-following architecture has a much worse scaling trend with N or x_0 than that in symmetric bidirectional architecture, no matter if the controller is linear or nonlinear, and that (ii) the nonlinear controller performs better than the linear controller in the predecessor-following architecture (Figures 4(a) and 5(a)), whereas it performs similarly or worse in the symmetric bidirectional architecture (Figures 4(b) and 5(b)).

Copyright © 2012 John Wiley & Sons, Ltd.

DOI: 10.1002/rnc

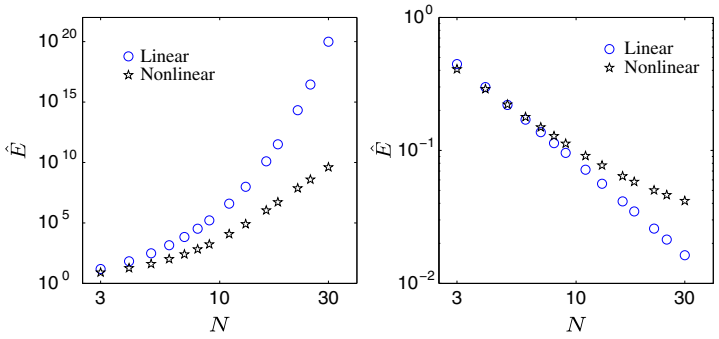

(a) Predecessor-following (b) Symmetric bidirectional

Figure 4. Comparison of $\hat{E}$ between linear and nonlinear controllers as a function of N. The measure E is estimated by numerically evaluating the integral in (12) for $T = 10^4$ s. The initial condition of the first agent used is $x_0 = 10$.

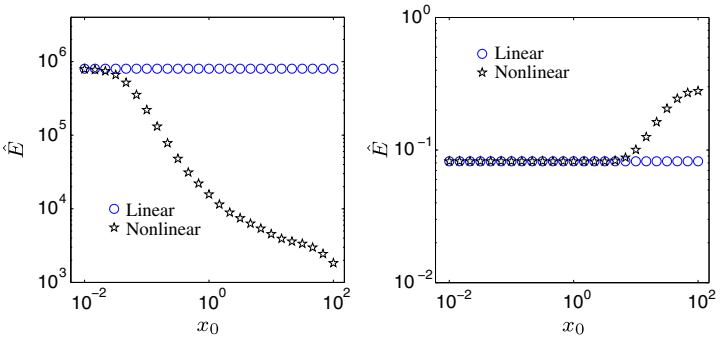

(a) Predecessor-following (b) Symmetric bidirectional

Figure 5. Comparison of $\hat{E}$ between linear and nonlinear controllers for a network of $N = 10$ agents as a function of initial conditions x_0. The measure $\hat{E}$ is estimated by numerically evaluating the integral in (12) for $T = 10^4$ s.

Table I. Comparison of transient performances between the two architectures.

	Predecessor following	Symmetric bidirectional
Convergence rate	Good	Bad
Transient energy	Bad	Good

3.4. Design guidelines based on transient response

On the basis of the numerical and analytical results, the comparisons of performance are summarized in Tables I and II. It follows that the predecessor-following architecture has a faster convergence rate (good) but much higher *integral of transient energy* E (bad) compared with the symmetric bidirectional architecture. These conclusions hold irrespective of whether the controller is linear or nonlinear (Figures 2–5). In fact, the transients are so large with the predecessor-following architecture that it is very likely to lead to collisions even for small initial errors. So if a design choice is to be made between the two architectures, the symmetric bidirectional should be chosen. Within the bidirectional architecture, the linear controller seems to perform slightly better than the nonlinear one, so the linear controller should be chosen. If, for some reason, the predecessor-following architecture has to be used, the nonlinear control law should be used because it clearly outperforms the linear one in terms of transient energy.

Copyright © 2012 John Wiley & Sons, Ltd.

DOI: 10.1002/rnc

Table II. Comparison of transient performances between linear and nonlinear controllers.

	Linear controller	Nonlinear controller
Predecessor following	Bad	Good
Symmetric bidirectional	Good	Bad

4. ROBUSTNESS (SENSITIVITY TO EXTERNAL DISTURBANCES)

In this section, we study the sensitivity of the network to external disturbances. Specifically, we examine appropriate gains from (i) a disturbance on the first agent $w_1 \in \mathbb{R}$ to the position tracking error of the last agent $\tilde{p}_N \in \mathbb{R}$ and from (ii) disturbances acting on all agents $w \in \mathbb{R}^N$ to the position tracking errors of all agents $\tilde{p} \in \mathbb{R}^N$. Both sinusoidal and random disturbances are considered. For the first scenario, we consider the metric *first-to-last amplification factor* (A_{FTL}), defined as the L_2 gain from input w_1 to output $\tilde{p}_N$:

$$A_{\mathrm{FTL}}^{\text{linear or nonlinear}} = \sup \frac{\|\tilde{p}_N\|_{\mathcal{L}_2(\tau)}}{\|w_1\|_{\mathcal{L}_2(\tau)}}, \tag{14}$$

where the $\mathcal{L}_2$ norm in the aforementioned expression is defined in the extended space [34], that is, $\|e\|_{\mathcal{L}_2(\tau)} := \sqrt{\int_0^\tau \|\mathrm{e}(t)\|^2 \,\mathrm{d}t}$ for a large but finite τ. In the linear case, denoting by $G_{\mathrm{FTL}}(s)$ the SISO transfer function from w_1 to $\tilde{p}_N$, this is the same as the H_∞ norm of $G_{\mathrm{FTL}}(s)$ [34], that is,

$$A_{\mathrm{FTL}}^{\text{linear}} = \max_\omega |G_{\mathrm{FTL}}(j\omega)| = |G_{\mathrm{FTL}}(j\omega_{\mathrm{p}})|, \text{ where } \omega_{\mathrm{p}} := \arg\max_\omega |G_{\mathrm{FTL}}(j\omega)| \tag{15}$$

and where we have assumed for the moment that the maximum is achieved at a finite frequency. The justification will be provided later. In the nonlinear case, we use the following quantity as a conservative estimate of the amplification factor:

$$\hat{A}_{\mathrm{FTL}}^{\text{nonlinear}} = \frac{\|\tilde{p}_N\|_{\mathcal{L}_2(\tau)}}{\|w_1\|_{\mathcal{L}_2(\tau)}}, \tag{16}$$

where $w_1 = a_1 \sin(\omega_{\mathrm{p}} t)$, a_1 is a positive constant, and ω_{p} is the peak frequency for the linear case that is defined in (15).

For the second scenario (effect of disturbances acting on every agent on their position tracking errors), we define the *all-to-all amplification factor* A_{ATA} as the L_2 gain from the vector of disturbances $w(t) = [w_1(t), \cdots, w_N(t)]$ to the position tracking error vector $\tilde{p}(t) = [\tilde{p}_1(t), \cdots, \tilde{p}_N(t)]$:

$$A_{\mathrm{ATA}}^{\text{linear or nonlinear}} = \sup \frac{\|\tilde{p}\|_{\mathcal{L}_2(\tau)}}{\|w\|_{\mathcal{L}_2(\tau)}}. \tag{17}$$

In the linear case, this is the H_∞ norm of the MIMO transfer function $G_{\mathrm{ATA}}(s)$ from w to $\tilde{p}$:

$$A_{\mathrm{ATA}}^{\text{linear}} = \max_\omega \sigma_{\max}(G_{\mathrm{ATA}}(j\omega)) = \sigma_{\max}(G_{\mathrm{ATA}}(j\omega_{\mathrm{p}})),$$

where we have assumed the maximum is achieved, $\omega_{\mathrm{p}} := \arg\max_\omega \sigma_{\max}(G_{\mathrm{ATA}}(j\omega))$, and $\sigma_{\max}$ denotes the maximum singular value. In the nonlinear case, evaluating $A_{\mathrm{ATA}}^{\text{nonlinear}}$ is intractable, so we use following conservative estimate:

$$\hat{A}_{\mathrm{ATA}}^{\text{nonlinear}} := \frac{\|\tilde{p}\|_{\mathcal{L}_2(\tau)}}{\|w\|_{\mathcal{L}_2(\tau)}}, \tag{18}$$

where $w = [a_1 \sin(\omega_{\mathrm{p}} t + \theta_1), \cdots, a_N \sin(\omega_{\mathrm{p}} t + \theta_N)]$ and $a = [a_1, \cdots, a_N]$ and $\theta = [\theta_1, \cdots, \theta_N]$ are the parameters that achieve the $\mathcal{L}_2$ norm in the linear case. The choice of these parameters is given in Theorem 4 and Corollary 1. Note from (14), (16), (17), and (18) that the estimates for the nonlinear case are lower bounds: $\hat{A}_{\mathrm{FTL}}^{\text{nonlinear}} \leqslant A_{\mathrm{FTL}}^{\text{nonlinear}}$ and $\hat{A}_{\mathrm{ATA}}^{\text{nonlinear}} \leqslant A_{\mathrm{ATA}}^{\text{nonlinear}}$.

Copyright © 2012 John Wiley & Sons, Ltd.

DOI: 10.1002/rnc

We also examine the effect of random disturbances. Specifically, let $w(t)$ in the closed-loop dynamics (8) be a scalar (or vector) of white noise with zero mean and autocorrelation function $E[w(t)w(t+\tau)^{\mathrm{T}}] = \sigma_0\delta(\tau)I, \forall\, t, \forall\, \tau$, where σ_0 is a constant, $\delta(\tau)$ is the Dirac delta function, and I is the identity matrix with appropriate dimension. Similar to sinusoidal disturbances, we define the following two metrics (i) *first-to-last ratio* and (ii) *all-to-all ratio*:

$$R_{\mathrm{FTL}}^{\text{linear or nonlinear}} := \lim_{t\to\infty} \frac{\sqrt{E(\tilde{p}_N^2(t))}}{\sigma_0}, \quad R_{\mathrm{ATA}}^{\text{linear or nonlinear}} := \lim_{t\to\infty} \frac{\sqrt{E(\tilde{p}(t)^{\mathrm{T}}\tilde{p}(t))}}{\sigma_0}, \tag{19}$$

where $E(.)$ denotes the expected value and we have assumed the aforementioned limits exist. Notice that, in the linear case, the aforementioned ratios are exactly the H_2 norms of the appropriate transfer functions from the white noise disturbances to the position tracking errors. The steady-state covariance matrix of the state $\tilde{p}(t)$ of the system (9) that is driven by a white noise process $w(t)$ is given by solution P of the following Lyapunov equation [35, Chapter 4]:

$$AP + PA^{\mathrm{T}} = -Q,$$

where $Q = \sigma_0 BB^{\mathrm{T}}$, and B is the appropriate input matrix given in (9). Because A is Hurwitz, it guarantees the limit in (19) exists [35]. The steady-state expectations $E(\tilde{p}_N^2(t))$ and $E(\tilde{p}(t)^{\mathrm{T}}\tilde{p}(t))$ given in (19) can be obtained by extracting the second last diagonal entry of P and summing the odd diagonal entries of P respectively, which yields

$$R_{\mathrm{FTL}}^{\mathrm{linear}} = \frac{\sqrt{P(2N-1,2N-1)}}{\sigma_0}, \quad R_{\mathrm{ATA}}^{\mathrm{linear}} = \frac{\sqrt{\sum_{i=1}^{N} P(2i-1,2i-1)}}{\sigma_0}. \tag{20}$$

It should be pointed out that these results are not as analytical as the results in [29, 30, 36]. Our study of random disturbances with linear control is closely related to the works by Bamieh, Jovanovic, and their coworkers [29, 30]. They derived scaling laws of all-to-all ratio for both predecessor-following and symmetric bidirectional architectures, which are similar to the scaling laws of H_∞ norms established in this paper (see Remark 2 for more details).

For the nonlinear controllers as well as linear controllers, we use the following estimate of the ratio defined in (19), which can be computed from simulation data:

$$\hat{R}_{\mathrm{FTL}}^{\text{linear or nonlinear}} := \frac{\sqrt{E(\tilde{p}_N^2(T))}}{\sigma_0}, \quad \hat{R}_{\mathrm{ATA}}^{\text{linear or nonlinear}} := \frac{\sqrt{E(\tilde{p}(T)^{\mathrm{T}}\tilde{p}(T))}}{\sigma_0}, \tag{21}$$

where T is sufficiently large such that the transients die out. Monte Carlo simulations are used to estimate the first-to-last and all-to-all ratios. For example, to compute the first-to-last ratio for the predecessor-following architecture with nonlinear controller, the noise-driven system (6) is converted into a standard stochastic differential equation form:

$$\begin{aligned} \mathrm{d}\tilde{p}_1 &= \dot{\tilde{p}}_1\mathrm{d}t, \quad \mathrm{d}\dot{\tilde{p}}_1 = -f(\tilde{p}_1)\mathrm{d}t - g(\dot{\tilde{p}}_1)\mathrm{d}t + \sigma_0\mathrm{d}W(t), \\ \mathrm{d}\tilde{p}_i &= \dot{\tilde{p}}_i\mathrm{d}t, \quad \mathrm{d}\dot{\tilde{p}}_i = -f(\tilde{p}_i - \tilde{p}_{i-1})\mathrm{d}t - g(\dot{\tilde{p}}_i - \dot{\tilde{p}}_{i-1})\mathrm{d}t, \end{aligned} \tag{22}$$

where $\tau = 2, \ldots, N$ and $W(t)$ is a standard Wiener process. Sample paths of the states are computed by using the Euler–Maruyama method to numerically integrate the stochastic differential equation (22) [37]. The metric $\hat{R}_{\mathrm{FTL}}^{\mathrm{nonlinear}}$ is now estimated by performing appropriate averaging over a large number of simulations, after letting each simulation proceed sufficiently long to allow transients to die out.

4.1. Sensitivity to disturbance with linear control

As stated earlier, analytical results on the sensitivity to disturbances are possible only for the linear case. The first result is on the sensitivity of the predecessor-following architecture with linear control.

Copyright © 2012 John Wiley & Sons, Ltd.

DOI: 10.1002/rnc

Theorem 4
Consider a 1-D network of N double-integrator agents with predecessor-following architecture. With linear controllers $f(x) = k_0 x$ and $g(x) = b_0 x$ in (3), the first-to-last amplification $A_{\mathrm{FTL}}^{\mathrm{linear}}$ and the all-to-all amplification $A_{\mathrm{ATA}}^{\mathrm{linear}}$ satisfy

$$\beta_1 \alpha^{N-1} \leqslant A_{\mathrm{FTL}}^{\mathrm{linear}} \leqslant \beta_2 \alpha^{N-1}, \quad \beta_1 \alpha^{N-1} \leqslant A_{\mathrm{ATA}}^{\mathrm{linear}} \leqslant \frac{\beta_2(\alpha^N - 1)}{\alpha - 1},$$

where $\alpha = |T(j\omega_T)| > 1$, $\beta_1 = |S(j\omega_T)|$, and $\beta_2 = |S(j\omega_S)|$, in which $T(s) = \frac{b_0 s + k_0}{s^2 + b_0 s + k_0}$, $S(s) = \frac{1}{s^2 + b_0 s + k_0}$, and ω_T and ω_S are the peak frequencies of $T(s)$ and $S(s)$, respectively.

Furthermore, when $N \gg 1$,

$$A_{\mathrm{FTL}}^{\mathrm{linear}} \approx \beta_1 \alpha^{N-1}, \qquad A_{\mathrm{ATA}}^{\mathrm{linear}} \approx \beta_1 \sqrt{\frac{(\alpha^{2N} - 1)}{\alpha^2 - 1}}, \qquad \omega_{\mathrm{p}} \approx \frac{\sqrt{\sqrt{k_0^4 + 2k_0^3 b_0^2} - k_0^2}}{b_0}. \tag{23}$$

Moreover, a sufficient condition for a disturbance $w = [w_1, \cdots, w_N] = [a_1 \sin(\omega t + \theta_1), \cdots, a_N \sin(\omega t + \theta_N)]$ to yield the worst amplification factors is $a = [a_1, \cdots, a_N] = [a_1, 0, \cdots, 0]$, where a_1 is an arbitrary constant and $\omega = \omega_{\mathrm{p}}$, $\theta = [\theta_1, \cdots, \theta_N] = 0$.

The proof of this theorem is omitted here, because it is similar to the proof of Lemma 1 in [14]. The interested reader can find a detailed proof in [38].

The next theorem is the corresponding result for the symmetric-bidirectional architecture.

Theorem 5
Consider a 1-D network of N double-integrator agents with symmetric bidirectional architecture. With linear controller $f(x) = k_0 x$ and $g(x) = b_0 x$ in (4), the first-to-last and all-to-all amplifications satisfy

$$\left(\frac{16}{\pi^3 b_0 \sqrt{k_0}}\right) N \leqslant A_{\mathrm{FTL}}^{\mathrm{linear}} \leqslant \left(\frac{\pi^3 + 18\pi}{12 b_0 \sqrt{2k_0}}\right) N, \text{ when } N \gg 1,$$
$$\left(\frac{1}{b_0 \sqrt{k_0} \pi^3}\right) (2N+1)^3 \leqslant A_{\mathrm{ATA}}^{\mathrm{linear}} \leqslant \left(\frac{1}{4 b_0 \sqrt{2k_0}}\right) (2N+1)^3, \quad \forall\, N.$$

Furthermore, when $N \gg 1$, the all-to-all amplification and its peak frequency are asymptotically

$$A_{\mathrm{ATA}}^{\mathrm{linear}} \approx \frac{8N^3}{\sqrt{k_0} b_0 \pi^3}, \quad \omega_{\mathrm{p}} \approx \frac{\sqrt{k_0}\pi}{2N}.$$

The asymptotic formulae for the first-to-last amplification and its peak frequency with symmetric bidirectional architecture are conjectured as follows. The argument for the conjecture is given in the end of the Appendix.

Conjecture 1
Assume the conditions of Theorem 5 hold. When $N \gg 1$, the first-to-last amplification and the peak frequency of the 1-D network are asymptotically

$$A_{\mathrm{FTL}}^{\mathrm{linear}} \approx \frac{8N}{\sqrt{k_0} b_0 \pi^2}, \quad \omega_{\mathrm{p}} = \omega_1 \approx \frac{\sqrt{k_0}\pi}{2N}.$$

The following result is a corollary of Theorem 5; it provides sufficient conditions for an input to achieve the $\mathcal{L}_2$ gain in the all-to-all scenario.

Copyright © 2012 John Wiley & Sons, Ltd.

DOI: 10.1002/rnc

Corollary 1
Assume the conditions of Theorem 5 hold. If the disturbance input satisfies $w = [w_1, \cdots, w_N] = v_1 \sin(\omega_1 t)$, where v_1 and ω_1, given in (A.11) and (A.15), respectively, are the eigenvector and the peak frequency corresponding to the principal eigenvalue λ_1 of L given in (A.9), then

$$A_{\mathrm{ATA}}^{\mathrm{linear}} = \frac{\|\tilde{p}\|_{\mathcal{L}_2(\tau)}}{\|w\|_{\mathcal{L}_2(\tau)}}.$$

The aforementioned corollary indicates that a sufficient condition for a disturbance $w = [w_1, \cdots, w_N] = [a_1 \sin(\omega t + \theta_1), \cdots, a_N \sin(\omega t + \theta_N)]$ to yield the all-to-all amplification factor for the symmetric bidirectional architecture is $a = [a_1, \cdots, a_N] = v_1$, $\omega = \omega_1$, and $\theta = [\theta_1, \cdots, \theta_N] = 0$. This result will be used to compute the estimate of all-to-all amplification factor $\hat{A}_{\mathrm{ATA}}^{\mathrm{nonlinear}}$ for nonlinear controllers, which is defined in (14).

Remark 2
On the basis of the analytical results in Theorems 4 and 5 (and Conjecture 1), we summarize the robustness results in Table III. We observe that symmetric bidirectional architecture has much better robustness than predecessor-following architecture. In particular, the first-to-last amplification scales geometrically in N as $O(\alpha^N), \alpha > 1$, for predecessor-following architecture but only linearly in N as $O(N)$ for symmetric bidirectional architecture. The all-to-all amplification scales as $O(\alpha^N)$ for predecessor-following architecture, whereas it scales as $O(N^3)$ for symmetric bidirectional architecture. Similar to the results on H_∞ norms established in this paper, it is worthy to mention that, with predecessor-following architecture, the 'all-to-all' ratio/H_2 norm of the 1-D network also scales exponentially with the number of agents N, even with absolute velocity feedback [30], although we consider in this paper the relative velocity feedback case. For the symmetric bidirectional architecture, Bamieh *et al.* showed in [29] that the 'all-to-all' ratio/H_2 norm scales only as $O(N^3)$.

4.2. Numerical comparison of sensitivity to disturbances between linear and nonlinear controllers

In this section, we present robustness metrics of the 1-D network with linear and nonlinear controllers empirically estimated using numerical computations. The analytical predictions of the performance metrics for the linear controllers are also presented to verify these predictions. The controllers used are the ones given by (13).

Figure 6 shows the first-to-last amplification factor as a function of N: Figure 6(a) is for predecessor following and Figure 6(b) is for symmetric bidirectional. The following observations are made. (i) The lower and upper bounds and asymptotic formulae derived are quite accurate, especially for the predecessor-following case. For the symmetric bidirectional architecture, Conjecture 1 is quite accurate. (ii) In the predecessor-following architecture, the growth of the first-to-last amplification factor with respect to N is much slower with the nonlinear controller than with the linear controller, as readily seen in Figure 6(a). In the symmetric bidirectional architecture, there is little difference between the two controllers for this sinusoidal disturbance, as seen from Figure 6(b). (iii) Comparing Figure 6(a) and (b), we see that the symmetric bidirectional architecture has a much smaller first-to-last amplification factor than the predecessor-following architecture, when the controller is linear. However, when nonlinear controller is applied, the symmetric bidirectional architecture has a slightly worse scaling trend than the predecessor-following case. The same conclusions can be drawn to the case of all-to-all amplification factor, whose numerical results are shown in Figure 7.

Table III. Comparison of robustness performances between the two architectures.

	Predecessor following	Symmetric bidirectional
First-to-last amplification	Bad ($O(\alpha^N), \alpha > 1$)	Good ($O(N)$)
All-to-all amplification	Bad ($O(\alpha^N), \alpha > 1$)	Good ($O(N^3)$)

Copyright © 2012 John Wiley & Sons, Ltd.

DOI: 10.1002/rnc

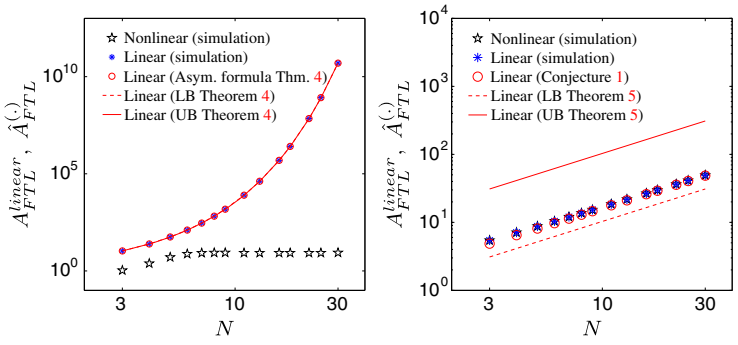

(a) Predecessor-following (b) Symmetric bidirectional

Figure 6. First-to-last amplification: sinusoidal disturbances. Comparison of first-to-last amplification factor with linear and nonlinear controllers. The sinusoidal disturbance on the first agent used is $0.1\sin(\omega_{\mathrm{p}}t)$. LB and UB stand for 'lower bound' and 'upper bound', respectively.

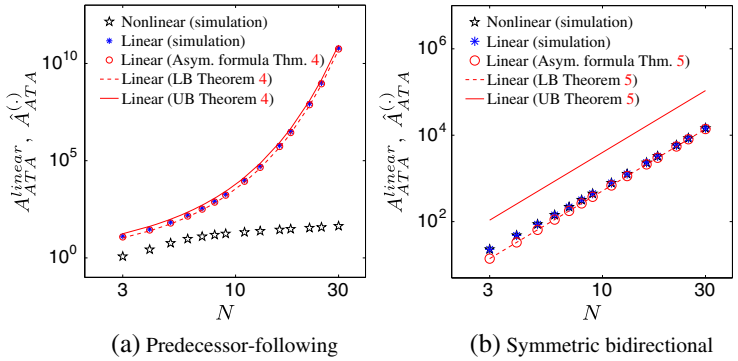

(a) Predecessor-following (b) Symmetric bidirectional

Figure 7. All-to-all amplification: sinusoidal disturbances. Comparison of all-to-all amplification factor with linear and nonlinear controllers. The sinusoidal disturbances used is $v_1\sin(\omega_{\mathrm{p}}t)$, where v_1 is the first eigenvector of L given in (A.11). LB and UB stand for 'lower bound' and 'upper bound', respectively.

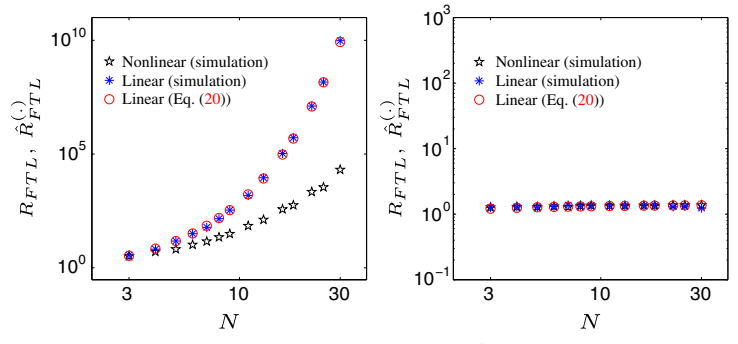

(a) Predecessor-following (b) Symmetric bidirectional

Figure 8. First-to-last ratio: random disturbance ($\sigma_0 = 1$), for both linear and nonlinear controllers.

To examine the effect of random disturbances, we compute the estimate $\hat{R}$ that is defined in (21) for $T = 3000$ s, through Monte Carlo simulations for both linear and nonlinear cases. For the first-to-last ratio, Figure 8 shows $\hat{R}_{\mathrm{FTL}}$ versus N for a fixed σ_0, whereas Figure 9 shows $\hat{R}_{\mathrm{FTL}}$ versus σ_0, the strength of the noise, for a fixed N. Numerical and analytical (20) results on the all-to-all ratio are shown in Figures 10 and 11. The conclusion of robustness to random noise that drawn from Figures 8–11 is the same as that for robustness to sinusoidal disturbances. We omit the discussion because of space limit.

Copyright © 2012 John Wiley & Sons, Ltd.

DOI: 10.1002/rnc

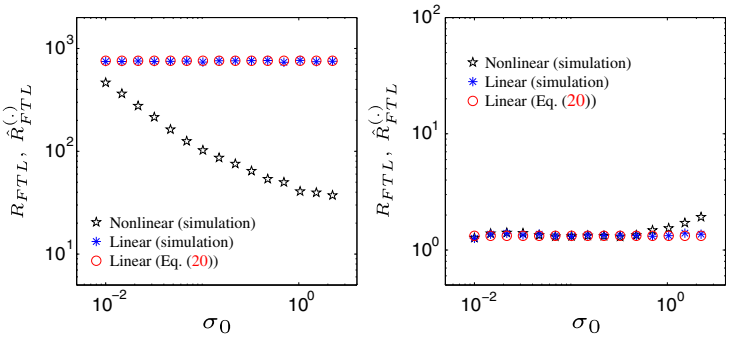

(a) Predecessor-following (b) Symmetric bidirectional

Figure 9. First-to-last ratio: random disturbances. Comparison of the ratios R_{FTL} and $\hat{R}_{\mathrm{FTL}}$ of a network of 10 agents as a function of the standard deviation σ_0 of the white noises.

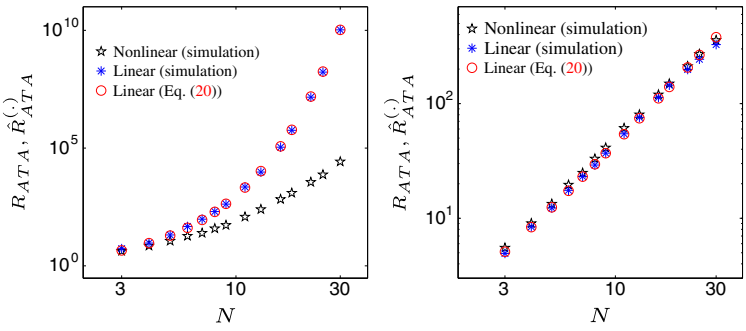

(a) Predecessor-following (b) Symmetric bidirectional

Figure 10. All-to-all ratio: random disturbances. Comparison of the ratios R_{ATA} and $\hat{R}_{\mathrm{ATA}}$ as a function of the number of agents N with white noise disturbances. The value of σ_0 used is 1.

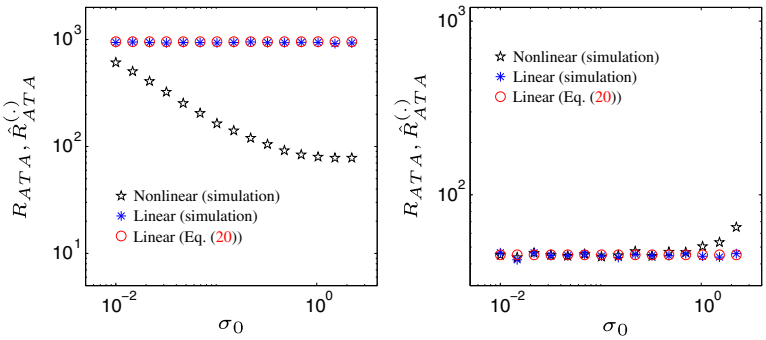

(a) Predecessor-following (b) Symmetric bidirectional

Figure 11. All-to-all ratio: random disturbances. Comparison of the ratios R_{ATA} and $\hat{R}_{\mathrm{ATA}}$ of a platoon of 10 agents as a function of the standard deviation σ_0 of the white noises.

4.3. Design guidelines based on robustness

On the basis of the empirical as well as the analytical results, the robustness performance results are summarized in Tables III and IV. A few broad conclusions that are useful for making design choices can be arrived at. (i) By comparing part (a) with part (b) for Figures 8–11, we conclude that the predecessor-following architecture has poorer performance compared with the symmetric bidirectional one, and the difference becomes more pronounced as N increases. Moreover, this conclusion holds irrespective of whether the disturbance is sinusoidal or random and whether the

Copyright © 2012 John Wiley & Sons, Ltd.

DOI: 10.1002/rnc

Table IV. Comparison of robustness performances between linear and nonlinear controllers.

	Linear controller	nonlinear controller
Predecessor following	Bad	Good
Symmetric bidirectional	Good	Bad

first-to-last ratio or the all-to-all ratio is used as a metric of robustness. (ii) If symmetric bidirectional architecture is indeed used, both the linear and nonlinear control laws have almost identical robustness. The only exception is when the strength of the disturbance is large, in which case, the nonlinear control law performs poorly compared with the linear one. Thus, a designer can use the linear control law because of its simplicity without losing performance. Because actuator saturation will be present in practice, the resulting closed-loop system even with a linear control law will be closer to the nonlinear system studied here. The previous observation therefore tells us that the symmetric bidirectional architecture is robust to modeling errors as well and therefore preferable from a practical standpoint. (iii) If the predecessor architecture is to be used because of other constraints such as cost, the nonlinear control law has better robustness to disturbance than its linear counterpart; see part (a) of Figures 8–11. Therefore, in this case, the nonlinear controller should be used.

5. SUMMARY

We studied the stability and robustness of large 1-D networks of double-integrator agents for two different decentralized architectures: predecessor following and symmetric bidirectional. Both linear and nonlinear controllers with certain sector nonlinearities were examined. For the linear case, we obtained exact formulae for convergence rates of the closed loop, whereas for the nonlinear case, closed-loop stability was proved. It was shown that the predecessor-following architecture with linear control has much faster convergence rate than the symmetric bidirectional architecture, but it suffers from high algebraic growth of initial errors. To compare performance with the nonlinear controller for which convergence rate could not be computed, an 'integral of transient energy' measure was proposed. Simulations showed that the symmetric bidirectional architecture has a better transient performance than the predecessor-following one, whether the controller is linear or nonlinear.

The robustness (sensitivity to external disturbances) of the closed loop is studied through two metrics, called the first-to-last amplification factor and the all-to-all amplification factor (called ratios instead of amplification factors when the disturbance is random instead of sinusoidal). In case of linear control, we derived scaling laws of the amplification factors of the 1-D network with respect to the number of agents for both architectures. For the nonlinear control case, the amplification factors were examined by extensive numerical simulations. The overall conclusion derived from a mix of analysis and simulations was that the symmetric bidirectional architecture's performance scales with N much better than that of the predecessor-following architecture. Simulations show that, in the case of the predecessor-following architecture, a class of saturation-type nonlinear controllers perform better compared with the linear control, both in terms of transient performance and sensitivity to external disturbances.

It should be noticed that the conclusions—and design guidelines—drawn from robustness considerations are consistent with the design guidelines drawn purely from transient response considerations; compare with Sections 4.3 and 3.4. Another important conclusion of these studies is the following: architecture has a more profound impact on performance than linearity or nonlinearity of the plant dynamics/control. The symmetric bidirectional architecture is seen to perform better than the predecessor-following architecture in almost all cases, with linear or nonlinear control, for various metrics of performance, and with sinusoidal or random disturbance. The only exception is convergence rate. Everything else being equal, the predecessor-following architecture has a faster convergence rate than the symmetric bidirectional. However, this comes with the

Copyright © 2012 John Wiley & Sons, Ltd.

DOI: 10.1002/rnc

associated cost of higher peak transients and higher transient energy, so that, with the predecessor-following architecture, collisions between agents can be avoided only if the initial spacial errors are extremely small.

Some of the simplifying assumptions made in this paper for the ease of exposition can be removed without much technical difficulty. Here, we have limited ourselves to a *homogeneous* network: each agent in the network has the same open-loop dynamics and uses the same control law. Convergence rate results in the linear case remain the same asymptotically (for large N) even in the case of a *heterogeneous* network, in which the masses and control gains vary from one agent to another. It was shown in [39] that, in the linear symmetric bidirectional case, heterogeneity in agent masses and control gains do not affect the asymptotic scaling (with N) of the convergence rate; they only change the coefficient. The nonlinear stability analysis in this paper can also be extended in a straightforward manner to the heterogeneous network. The linear stability results of this paper can be extended to formations with more general information graphs—compared with the 1-D formation studied here—by using the methodology of [38, 40].

The scaling laws for the convergence rate and robustness metrics for the linear case can also be extended to a more general class of agent models and dynamic compensators. In particular, when the agent model $H(s)$ (transfer function from input to position) is not simply $1/s^2$ but $1/s^2 P(s)$, where $P(s)$ is a transfer function with $0 < P(0) < \infty$, the analysis can be carried out in a manner similar to that in [14] for the predecessor-following case and [23] for the symmetric bidirectional case. As shown in [23], the key attribute of the model that determines robustness scaling is the number of integrators in the loop; additional dynamics only affect the high-frequency portion, whereas the robustness scaling with N is determined only by the low-frequency portion of the frequency response of the loop transfer function. The reason for the importance of the low-frequency band is the unbounded gain and -180° phase of $1/s^2$ at dc. As a result, the worst-case amplification occurs at a progressively lower frequency as N increases. Recall Theorem 5: the peak frequencies for the symmetric bidirectional case is $O(1/N)$.

It should be emphasized that the results for the symmetric architecture obtained here do not extend to the *asymmetric* case, in which an agent uses information from its predecessor (front neighbor) differently than the information from its follower (back neighbor). One can introduce a *mistuning parameter* $\epsilon \in [-1, 1]$ to quantify this asymmetry: $\epsilon = 0$ corresponds to the case of symmetric bidirectional case, whereas $\epsilon = 1$ corresponds to the predecessor-following architecture, with $0 < \epsilon < 1$ corresponding to a case when the front neighbor's information is weighted more heavily than that of the back neighbor and with $-1 < \epsilon < 0$ corresponding to the opposite. The difference between the two architectures established here already provides evidence that asymmetry has a nonnegligible effect. Recent works have shown that even small amount of asymmetry can have a huge impact, on both convergence rate [39, 41] and robustness in terms of, respectively, H_∞ norm [28] and H_2 norm [30]. It was shown in [28, 30, 39] that asymmetry can either significantly improve or deteriorate the system's convergence rate and robustness, depending on the choice of asymmetry. These works have studied the linear case. Analysis of stability with general asymmetric nonlinear control is an open problem. In fact, analysis of the sensitivity to disturbance with general asymmetric control (linear or nonlinear) is also an open problem.

APPENDIX

Proof of Theorem 1

For the predecessor-following architecture with linear controller, it follows from straightforward algebra that the state matrix A can be written as

$$A = \begin{bmatrix} A_1 & & & \\ A_2 & A_1 & & \\ & \ddots & \ddots & \\ & & A_2 & A_1 \end{bmatrix}, \quad A_1 = \begin{bmatrix} 0 & 1 \\ -k_0 & -b_0 \end{bmatrix}, \quad A_2 = \begin{bmatrix} 0 & 0 \\ k_0 & b_0 \end{bmatrix}. \tag{A.1}$$

Copyright © 2012 John Wiley & Sons, Ltd.

DOI: 10.1002/rnc

The state matrix A is a lower block triangular matrix, whose eigenvalues are determined by the block matrix A_1 on the diagonal. The eigenvalues of A_1 are $\frac{-b_0 \pm \sqrt{b_0^2 - 4k_0}}{2}$. Because there are N such block matrices on the diagonal of A, its eigenvalues have multiplicity N. Because the least stable eigenvalue is the one closest to the imaginary axis, it is given by $\mu_1 = \frac{-b_0 + \sqrt{b_0^2 - 4k_0}}{2}$, and this eigenvalue occurs with multiplicity N.

The result for the symmetric bidirectional architecture follows from Theorem 4 in [42] in a straightforward manner and is therefore omitted. □

The proof of Theorem 2 will use the following proposition.

Proposition 1
Consider the second-order autonomous system $\dot{y}_1 = y_2, \dot{y}_2 = -f(y_1 - u_1) - g(y_2 - u_2)$, where $y_1, y_2, u_1, u_2 \in \mathbb{R}$ and the odd functions $f, g : \mathbb{R} \to \mathbb{R}$ lie in the sectors $f \in [\varepsilon_1, K_1]$ and $g \in [\varepsilon_2, K_2]$, where $0 < \varepsilon_1 \leqslant K_1 < \infty$ and $0 < \varepsilon_2 \leqslant K_2 < \infty$. The origin of the unforced system (with $u(t) = [u_1(t), u_2(t)]^{\mathrm{T}} \equiv 0$) is globally exponentially stable (GES), and the system is input-to-state stable (ISS) with u as the input.

Proof of Proposition 1
First, we consider the unforced system with state $y = [y_1, y_2]^{\mathrm{T}}$:

$$\dot{y}_1 = y_2, \qquad \dot{y}_2 = -f(y_1) - g(y_2). \tag{A.2}$$

Consider the following Lyapunov function candidate:

$$V(y) = \frac{1}{2} y^{\mathrm{T}} P y + \gamma \int_0^{y_1} f(z)\mathrm{d}z, \tag{A.3}$$

where $P = \begin{bmatrix} 1 & 1 \\ 1 & \gamma \end{bmatrix}$ and $\gamma \geqslant \max\left\{1, \frac{1}{\varepsilon_2} + \frac{(1+K_2)^2}{\varepsilon_1 \varepsilon_2}\right\}$, which ensures that P is positive definite. From the Rayleigh–Ritz theorem [34], we have the inequality $\lambda_{\min}(P)\|y\|^2 \leqslant y^{\mathrm{T}} P y \leqslant \lambda_{\max}(P)\|y\|^2$, where $\lambda_{\min}(P) > 0$ and $\lambda_{\max}(P) > 0$ are the minimum and maximum eigenvalues of P, respectively. This shows that $V(y)$ is radially unbounded and satisfies the following:

$$V(y) \leqslant \frac{\lambda_{\max}(P)}{2}\|y\|^2 + \frac{\gamma K_1}{2} y_1^2 \leqslant \frac{\lambda_{\max}(P) + \gamma K_1}{2}\|y\|^2, \tag{A.4}$$

where the second inequality follows from the fact that the function $f(z)$ belongs to the sector $[\varepsilon_1, K_1]$. The derivative of V along the trajectory of (A.2) is given by

$$\begin{aligned}
\dot{V} &= y^{\mathrm{T}} P \dot{y} + \gamma f(y_1) y_2 = -y_1 f(y_1) - \gamma y_2 g(y_2) + y_2^2 + y_1 y_2 - y_1 g(y_2) \\
&\leqslant -\varepsilon_1 y_1^2 - (\gamma \varepsilon_2 - 1) y_2^2 + (1 + K_2)|y_1||y_2| \\
&\leqslant -\frac{1}{2}\left(\varepsilon_1 y_1^2 + (\gamma \varepsilon_2 - 1) y_2^2\right) - \frac{1}{2}\left[\varepsilon_1 y_1^2 - 2(1 + K_2)|y_1||y_2| + (\gamma \varepsilon_2 - 1) y_2^2\right] \\
&\leqslant -\frac{1}{2}\left(\varepsilon_1 y_1^2 + (\gamma \varepsilon_2 - 1) y_2^2\right) \leqslant -\frac{1}{2}\min\{\varepsilon_1, (\gamma \varepsilon_2 - 1)\}\|y\|^2,
\end{aligned} \tag{A.5}$$

where the second last inequality follows from $\gamma \geqslant \max\left\{1, \frac{1}{\varepsilon_2} + \frac{(1+K_2)^2}{\varepsilon_1 \varepsilon_2}\right\}$, upon a completion of squares. Because V is radially unbounded and satisfies (A.4), it follows from (A.5) that the origin $y = 0$ of (A.2) is GES. Because the functions f and g are assumed to be smooth enough, the ISS property follows from the fact that a GES system with input u is ISS [34, Lemma 4.6]. □

Copyright © 2012 John Wiley & Sons, Ltd.

DOI: 10.1002/rnc

Proof of Theorem 2

We first consider the subsystem consisted of only the first agent. Its closed-loop dynamics can be written as follows by using the fact $\tilde{p}_0 = \dot{\tilde{p}}_0 \equiv 0$:

$$\ddot{\tilde{p}}_1 = -f(\tilde{p}_1 - \tilde{p}_0) - g\left(\dot{\tilde{p}}_1 - \dot{\tilde{p}}_0\right) \quad \Rightarrow \quad \ddot{\tilde{p}}_1 = -f(\tilde{p}_1) - g\left(\dot{\tilde{p}}_1\right) \quad \Rightarrow \quad x^{(1)} = \mathbf{f}_1\left(x^{(1)}\right),$$

where $x^{(1)} = [\tilde{p}_1, \dot{\tilde{p}}_1]^{\mathrm{T}}$. From Proposition 1, we have that the origin $x^{(1)} = 0$ of the subsystem $x^{(1)} = \mathbf{f}_1(x^{(1)})$ is GES. Next, we consider the subsystem consisted of the first two agents. Its closed-loop dynamics can be written as

$$\begin{cases} \ddot{\tilde{p}}_1 = -f(\tilde{p}_1) - g\left(\dot{\tilde{p}}_1\right), \\ \ddot{\tilde{p}}_2 = -f(\tilde{p}_2 - \tilde{p}_1) - g\left(\dot{\tilde{p}}_2 - \dot{\tilde{p}}_1\right), \end{cases} \quad \Rightarrow \quad x^{(1+2)} = \mathbf{f}_{1+2}\left(x^{(1+2)}\right),$$

where $x^{(1+2)} = [\tilde{p}_1, \dot{\tilde{p}}_1, \tilde{p}_2, \dot{\tilde{p}}_2]^{\mathrm{T}}$. The aforementioned dynamics can be divided into two parts:

$$x^{(1+2)} = \mathbf{f}_{1+2}\left(x^{(1+2)}\right) \quad \Rightarrow \quad \begin{cases} x^{(1)} = \mathbf{f}_1\left(x^{(1)}\right), \\ x^{(2)} = \mathbf{f}_2\left(x^{(2)}, x^{(1)}\right), \end{cases} \tag{A.6}$$

where $x^{(2)} = [\tilde{p}_2, \dot{\tilde{p}}_2]^{\mathrm{T}}$. The unforced system $x^{(2)} = \mathbf{f}_2(x^{(2)}, 0)$ is given by

$$x^{(2)} = \mathbf{f}_1\left(x^{(2)}, 0\right) \quad \Rightarrow \quad \ddot{\tilde{p}}_2 = -f(\tilde{p}_2) - g\left(\dot{\tilde{p}}_2\right).$$

According to Proposition 1, the origin $x^{(2)} = 0$ of the unforced system $x^{(2)} = \mathbf{f}_2(x^{(2)}, 0)$ is GES, and it is ISS with $x^{(1)}$ as the input. We now invoke [34, Lemma 4.7]: the origin of the cascade system $x^{(1+2)} = \mathbf{f}_{1+2}(x^{(1+2)})$ given in (A.6) is GAS. We now prove that the origin of the whole system is GAS by induction. Suppose the origin $x^{(1+\cdots+N-1)} = 0$ of the subsystem consisted of the first $N-1$ agents $x^{(1+\cdots+N-1)} = \mathbf{f}_{1+\cdots+N-1}(x^{(1+\cdots+N-1)})$ is GAS; we consider the whole system, whose dynamics is given by

$$\dot{x} = \mathbf{f}(x) \quad \Rightarrow \quad x^{(1+\cdots+N)} = \mathbf{f}_{1+\cdots+N}\left(x^{(1+\cdots+N)}\right).$$

The aforementioned dynamics can be divided into two parts:

$$x^{(1+\cdots+N)} = \mathbf{f}_{1+\cdots+N}\left(x^{(1+\cdots+N)}\right), \quad \Rightarrow \quad \begin{array}{r} x^{(1+\cdots+N-1)} = \mathbf{f}_{1+\cdots+N-1}\left(x^{(1+\cdots+N-1)}\right), \\ x^{(N)} = \mathbf{f}_N\left(x^{(N)}, x^{(1+\cdots+N-1)}\right), \end{array} \tag{A.7}$$

The unforced system $x^{(N)} = \mathbf{f}_N(x^{(N)}, 0)$ is given by

$$x^{(N)} = \mathbf{f}_N\left(x^{(N)}, 0\right) \quad \Rightarrow \quad \ddot{\tilde{p}}_N = -f(\tilde{p}_N) - g(\dot{\tilde{p}}_N).$$

According to Proposition 1, the origin $x^{(N)} = 0$ of the unforced system $x^{(N)} = \mathbf{f}_N(x^{(N)}, 0)$ is GES, and it is ISS with $x^{(1+\cdots+N-1)}$ as the input. Invoking [34, Lemma 4.7] again, we see that the origin $x = x^{(1+\cdots+N)} = 0$ of the whole system whose dynamics is given in (A.7) is GAS. This completes the proof by induction. □

Proof of Theorem 3

For the 1-D network of double-integrator agents with symmetric bidirectional architecture, we consider the following Lyapunov function candidate, which is inspired by the one used in [25]:

$$V(x) = \sum_{i=1}^{N} \int_0^{\tilde{p}_i - \tilde{p}_{i-1}} f(z)\mathrm{d}z + \frac{1}{2}\sum_{i=1}^{N} \dot{\tilde{p}}_i^2,$$

where $x = [\tilde{p}_1, \dot{\tilde{p}}_1, \tilde{p}_2, \dot{\tilde{p}}_2, \cdots, \tilde{p}_N, \dot{\tilde{p}}_N]$. The derivative of V along the trajectory of (7) with $w_i = 0$ is

$$\dot{V} = \sum_{i=1}^{N} f(\tilde{p}_i - \tilde{p}_{i-1})(\dot{\tilde{p}}_i - \dot{\tilde{p}}_{i-1}) + \sum_{i=1}^{N} \dot{\tilde{p}}_i \ddot{\tilde{p}}_i = -\sum_{i=1}^{N} (\dot{\tilde{p}}_i - \dot{\tilde{p}}_{i-1}) g(\dot{\tilde{p}}_i - \dot{\tilde{p}}_{i-1}) \leqslant 0.$$

Copyright © 2012 John Wiley & Sons, Ltd.

DOI: 10.1002/rnc

If $\dot{V} = 0$, then we have $\dot{\tilde{p}}_i = 0$ for all i, because $g(z)$ satisfies $zg(z) > 0, \forall x \neq 0$ and $\dot{\tilde{p}}_0 = 0$, by definition. Asymptotic stability now follows from LaSalle's Invariance Principle. In addition, we have $V(x) \to \infty$ as $\|x\| \to \infty$. Therefore, the Lyapunov function V is radially unbounded, and we have global asymptotic stability. □

Proof of Theorem 5

Take the Laplace transform of the coupled-ODE model (7) and assume zero initial conditions; the transfer function from the disturbance $w = [w_1, \cdots, w_N]^{\mathrm{T}}$ to position error $\tilde{p} = [\tilde{p}_1, \cdots, \tilde{p}_N]^{\mathrm{T}}$ is given by

$$G(s) = \left(s^2 I + (b_0 s + k_0)L\right)^{-1}, \tag{A.8}$$

where I is the $N \times N$ identity matrix and L is given by

$$L = \begin{bmatrix} 2 & -1 & & & \\ -1 & 2 & -1 & & \\ & \ddots & \ddots & \ddots & \\ & & -1 & 2 & -1 \\ & & & -1 & 1 \end{bmatrix}. \tag{A.9}$$

Following Theorem 3.1 of [43], the eigenvalues of L and its corresponding orthonormal eigenvectors are given by

$$\lambda_\ell = 2 - 2\cos\left(\frac{(2\ell-1)\pi}{2N+1}\right) = 4\sin^2\left(\frac{(2\ell-1)\pi}{2(2N+1)}\right), \tag{A.10}$$

$$v_\ell = \frac{2}{\sqrt{2N+1}}\left[\sin\left(\frac{(2\ell-1)\pi}{2N+1}\right), \cdots, \sin\left(\frac{(2\ell-1)N\pi}{2N+1}\right)\right]^{\mathrm{T}}. \tag{A.11}$$

(i) *For the case of first-to-last amplification*, the transfer function G_{FTL} from disturbance w_1 on the first agent to the position error of the last agent $\tilde{p}_N$ is $G_{\mathrm{FTL}} = \phi_N^{\mathrm{T}} G(s)\phi_1$, where ϕ_i is the ith canonical basis vector of $\mathbb{R}^N$ whose ith entry is 1 and the rest are all 0's. Therefore,

$$\begin{aligned} G_{\mathrm{FTL}}(s) &= \phi_N^{\mathrm{T}} M(s^2 I + (b_0 s + k_0)\Lambda)^{-1} M^{\mathrm{T}} \phi_1 \\ &= \phi_N^{\mathrm{T}} M \begin{bmatrix} \frac{1}{s^2+\lambda_1 b_0 s+\lambda_1 k_0} & & \\ & \ddots & \\ & & \frac{1}{s^2+\lambda_N b_0 s+\lambda_N k_0} \end{bmatrix} M^{\mathrm{T}} \phi_1 \\ &= \frac{4}{2N+1}\sum_{\ell=1}^{N}\left(\sin\frac{(2\ell-1)N\pi}{2N+1}\sin\frac{(2\ell-1)\pi}{2N+1} G_\ell(s)\right), \end{aligned} \tag{A.12}$$

where $M = [v_1, v_2, \cdots, v_N]$ and $\Lambda = \mathrm{diag}(\lambda_1, \lambda_2, \cdots, \lambda_N)$ such that $L = M\Lambda M^{\mathrm{T}}$ and

$$G_\ell(s) := \frac{1}{s^2 + \lambda_\ell b_0 s + \lambda_\ell k_0}. \tag{A.13}$$

It can be shown using straightforward calculus that, for each eigenvalue λ_ℓ, the maximum amplitude and its peak frequency of $G_\ell(s)$ are as follows:

$$A_\ell := \max_\omega |G_\ell(j\omega)| = \begin{cases} \dfrac{2}{\lambda_\ell^{3/2} b_0 \sqrt{4k_0 - \lambda_\ell b_0^2}} & \text{if } \lambda_\ell \leqslant 2k_0/b_0^2, \\ \dfrac{1}{\lambda_\ell k_0} & \text{otherwise.} \end{cases} \tag{A.14}$$

Copyright © 2012 John Wiley & Sons, Ltd.

DOI: 10.1002/rnc

$$\omega_\ell := \arg\max |G_\ell(j\omega)| = \begin{cases} \dfrac{\sqrt{4\lambda_\ell k_0 - 2\lambda_\ell^2 b_0^2}}{2} & \text{if } \lambda_\ell \leqslant 2k_0/b_0^2, \\ 0 \quad \text{otherwise.} \end{cases} \tag{A.15}$$

From (A.10), $\lambda_1 < \lambda_2 < \cdots < \lambda_N$, which can be used to show by straightforward algebra that $A_1 > A_2 > \cdots > A_N$. For future use, we have from $\frac{2}{\pi}\theta \leqslant \sin\theta \leqslant \theta, \forall\ \theta \in [0, \frac{\pi}{2}]$, that

$$\frac{4(2\ell-1)^2}{(2N+1)^2} \leqslant \lambda_\ell \leqslant \frac{(2\ell-1)^2\pi^2}{(2N+1)^2}. \tag{A.16}$$

We first express $G_{\mathrm{FTL}}(s)$ in (A.12) as

$$G_{\mathrm{FTL}}(s) = T(s) + Z(s), \tag{A.17}$$

where

$$T(s) = \frac{4}{2N+1} \sin\frac{N\pi}{2N+1} \sin\frac{\pi}{2N+1} G_1(s), \tag{A.18}$$

$$Z(s) = \frac{4}{2N+1} \sum_{\ell=2}^{N} \left(\sin\frac{(2\ell-1)N\pi}{2N+1} \sin\frac{(2\ell-1)\pi}{2N+1} G_\ell(s) \right). \tag{A.19}$$

Now,

$$\sup_\omega |G_{\mathrm{FTL}}(j\omega)| \leqslant \sup_\omega |T(j\omega)| + \sup_\omega |Z(j\omega)| = |T(j\omega_1)| + \sup_\omega |Z(j\omega)|,$$
$$\sup_\omega |G_{\mathrm{FTL}}(j\omega)| \geqslant |T(j\omega_1) + Z(j\omega_1)| \geqslant |T(j\omega_1)| - |Z(j\omega_1)|,$$

where ω_1 is given in (A.15). Combining the aforementioned two inequalities, we obtain

$$|T(j\omega_1)| - |Z(j\omega_1)| \leqslant \sup_\omega |G(j\omega)| \leqslant |T(j\omega_1)| + \sup_\omega |Z(j\omega)|. \tag{A.20}$$

We now derive an upper bound for $\sup_\omega |Z(j\omega)|$. With the use of triangle inequality, it follows that (A.19) satisfies

$$\begin{aligned} \sup_\omega |Z(j\omega)| &\leqslant \frac{4}{2N+1} \sum_{\ell=2}^{N} \left(\sin\frac{(2\ell-1)N\pi}{2N+1} \sin\frac{(2\ell-1)\pi}{2N+1} \sup_\omega |G_\ell(j\omega)| \right) \\ &\leqslant \frac{4}{2N+1} \sum_{\ell=2}^{N} \left(\sin\frac{(2\ell-1)\pi}{2N+1} A_\ell \right) \leqslant \frac{4}{2N+1} \sum_{\ell=2}^{N} \frac{(2\ell-1)\pi}{2N+1} A_\ell, \end{aligned} \tag{A.21}$$

where the last inequality follows from the fact that $\sin\theta \leqslant \theta$ for $\theta \in [0, \pi/2]$ and $\frac{(2\ell-1)\pi}{2N+1} \in [0, \pi/2]$ for $2 \leqslant \ell \leqslant N$. From (A.14), we notice that, depending on whether $\lambda_\ell \leqslant 2k_0/b_0^2$ or not, the expressions of A_ℓ's are different. First, we have

$$\lambda_\ell \leqslant 2k_0/b_0^2 \quad \Rightarrow \quad \frac{1}{4k_0 - \lambda_\ell b_0^2} \leqslant \frac{1}{2k_0} \quad \text{and} \quad \lambda_\ell > 2k_0/b_0^2 \quad \Rightarrow \quad \frac{1}{\lambda_\ell} < \frac{b_0^2}{2k_0}. \tag{A.22}$$

Let N_c be in the index so that $\ell \leqslant N_c \Rightarrow \lambda_\ell \leqslant 2k_0/b_0^2$ and $\ell > N_c \Rightarrow \lambda_\ell > 2k_0/b_0^2$. The inequality in (A.21) can be written as

$$\begin{aligned} \sup_\omega |Z(j\omega)| &\leqslant \frac{4}{2N+1} \left(\sum_{\ell=2}^{N_c} \frac{(2\ell-1)\pi}{2N+1} \frac{2}{\lambda_\ell^{3/2} b_0 \sqrt{4k_0 - \lambda_\ell b_0^2}} + \sum_{\ell=N_c}^{N} \frac{(2\ell-1)\pi}{2N+1} \frac{1}{\lambda_\ell k_0} \right) \\ &\leqslant \frac{4}{(2N+1)^2} \sum_{\ell=2}^{N} \left(\frac{(2\ell-1)\pi}{\sqrt{2k_0} b_0} \frac{2}{\lambda_\ell^{3/2}} + (2\ell-1)\pi \frac{b_0^2}{2k_0^2} \right). \end{aligned} \tag{A.23}$$

Copyright © 2012 John Wiley & Sons, Ltd.

DOI: 10.1002/rnc

From (A.16), we have $\frac{1}{\lambda_\ell^{3/2}} \leqslant \frac{(2N+1)^3}{8(2\ell-1)^3}$. The inequality (A.23) becomes

$$\begin{aligned}\sup_\omega |Z(j\omega)| &\leqslant \frac{\pi(2N+1)}{\sqrt{2k_0}b_0}\sum_{\ell=2}^{N}\frac{1}{(2\ell-1)^2} + \frac{2b_0^2\pi}{k_0^2(2N+1)^2}\sum_{\ell=2}^{N}(2\ell-1)\\ &\leqslant \frac{\pi(2N+1)}{4\sqrt{2k_0}b_0}\sum_{\ell=2}^{\infty}\frac{1}{(\ell-1)^2} + \frac{2b_0^2\pi}{k_0^2(2N+1)^2}\sum_{\ell=2}^{N}(2\ell-1)\\ &\leqslant \frac{\pi(2N+1)}{4\sqrt{2k_0}b_0}\left(\frac{\pi^2}{6}-1\right) + \frac{2b_0^2\pi}{k_0^2(2N+1)^2}(N^2-1), \end{aligned} \tag{A.24}$$

where the last inequality follows from $\sum_{\ell=1}^{\infty}\frac{1}{\ell^2} = \frac{\pi^2}{6}$ and $\sum_{\ell=1}^{N}(2\ell-1) = N^2$. This proves an upper bound for $\sup_\omega |Z(j\omega)|$.

We now obtain an upper bound for $|T(j\omega_1)|$:

$$\begin{aligned}|T(j\omega_1)| &= \frac{4}{2N+1}\sin\frac{N\pi}{2N+1}\sin\frac{\pi}{2N+1}A_1 \leqslant \frac{4}{2N+1}\frac{\pi}{2N+1}A_1\\ &\leqslant \frac{4}{2N+1}\frac{\pi}{2N+1}\frac{2}{\lambda_1^{3/2}b_0\sqrt{4k_0-\lambda_1 b_0^2}} + \frac{4}{2N+1}\frac{\pi}{2N+1}\frac{1}{\lambda_1 k_0}\\ &\leqslant \frac{4\pi}{(2N+1)^2}\frac{(2N+1)^3}{4b_0\sqrt{2k_0}} + \frac{4\pi}{(2N+1)^2}\frac{b_0^2}{2k_0^2} \leqslant \frac{\pi(2N+1)}{b_0\sqrt{2k_0}} + \frac{2b_0^2\pi}{k_0^2(2N+1)^2}, \end{aligned} \tag{A.25}$$

Substituting inequalities (A.24) and (A.25) into (A.20), we obtain an upper bound for $\sup_\omega |G_{\mathrm{FTL}}(j\omega)|$:

$$\sup_\omega |G_{\mathrm{FTL}}(j\omega)| \leqslant \left(\frac{\pi^3+18\pi}{12b_0\sqrt{2k_0}}\right)N + c_1, \tag{A.26}$$

where c_1 is a constant independent of N.

To prove the lower bound for $|T(j\omega_1)|$, we first use the fact that $\frac{2}{\pi}\theta \leqslant \sin\theta, \forall\ \theta \in [0, \frac{\pi}{2}]$,

$$\begin{aligned}|T(j\omega_1)| &= \frac{4}{2N+1}\sin\frac{N\pi}{2N+1}\sin\frac{\pi}{2N+1}A_1\\ &\geqslant \frac{4}{2N+1}\frac{2}{\pi}\frac{N\pi}{2N+1}\frac{2}{\pi}\frac{\pi}{2N+1}A_1 \geqslant \frac{16N}{(2N+1)^3}A_1. \end{aligned} \tag{A.27}$$

For any fixed k_0 and b_0, when N is large, we have $\lambda_1 < 2k_0/b_0^2$, which implies

$$A_1 = \frac{2}{\lambda_1^{3/2}b_0\sqrt{4k_0-\lambda_1 b_0^2}} \geqslant \frac{1}{\lambda_1^{3/2}b_0\sqrt{k_0}} \geqslant \frac{1}{b_0\sqrt{k_0}}\frac{(2N+1)^3}{\pi^3}, \tag{A.28}$$

where the last inequality is obtained from (A.16). The inequality (A.27) now becomes

$$|T(j\omega_1)| \geqslant \frac{16N}{\pi^3 b_0\sqrt{k_0}}. \tag{A.29}$$

In addition, we have

$$\begin{aligned}|Z(j\omega_1)| &\leqslant \frac{4}{2N+1}\sum_{\ell=2}^{N}\left(\frac{(2\ell-1)\pi}{2N+1}|G_\ell(j\omega_1)|\right)\\ &\leqslant \frac{4}{2N+1}\sum_{\ell=2}^{N}\left(\frac{(2\ell-1)\pi}{2N+1}\frac{1}{\lambda_\ell k_0\sqrt{(1-\lambda_1/\lambda_2)^2}}\right).\end{aligned}$$

Copyright © 2012 John Wiley & Sons, Ltd.

DOI: 10.1002/rnc

From (A.16), we obtain that $\frac{1}{\lambda_\ell} \leqslant \frac{(2N+1)^2}{4(2\ell-1)^2}$, $\frac{\lambda_1}{\lambda_2} \leqslant \frac{\pi^2}{36}$. Thus, the aforementioned inequality can be simplified to

$$|Z(j\omega_1)| \leqslant 2c_2 \sum_{\ell=2}^{N} \left(\frac{(2\ell-1)}{(2N+1)^2} \frac{(2N+1)^2}{4(2\ell-1)^2} \right) \leqslant 2c_2 \sum_{\ell=2}^{N} \left(\frac{1}{(2\ell-1)} \right) \leqslant c_2 \sum_{\ell=1}^{N-1} \frac{1}{\ell},$$

where $c_2 = \frac{\pi}{2k_0\sqrt{(1-\pi^2/36)^2}}$ is a constant independent of N. Moreover, $\sum_{\ell=1}^{N-1} \frac{1}{\ell} = 1 + \sum_{\ell=2}^{N-1} \frac{1}{\ell} \leqslant 1 + \int_1^{N-1} \frac{1}{s}\, \mathrm{d}s$, and we have $\sum_{\ell=1}^{N-1} \frac{1}{\ell} \leqslant 1 + \ln(N-1)$. Thus, we have

$$|Z(j\omega_1)| \leqslant c_2 \ln(N-1) + c_2. \tag{A.30}$$

Substituting inequalities (A.30) and (A.29) into (A.20), we obtain a lower bound for $\sup_\omega |G_{\mathrm{FTL}}(j\omega)|$:

$$\sup_\omega |G_{\mathrm{FTL}}(j\omega)| \geqslant \frac{16N}{\pi^3 b_0 \sqrt{k_0}} - c_2 \ln(N-1) - c_2. \tag{A.31}$$

In addition, when N is large, the constants c_1 and c_2 and the $O(\ln(N-1))$ term are dominated by the $O(N)$ term; therefore, we ignore them in (A.26) and (A.31), respectively, and we obtain

$$\left(\frac{16}{\pi^3 b_0 \sqrt{k_0}} \right) N \leqslant A_{\mathrm{FTL}}^{\mathrm{linear}} \leqslant \left(\frac{\pi^3 + 18\pi}{12 b_0 \sqrt{2k_0}} \right) N.$$

(ii) *For the case of all-to-all amplification*, the transfer function from the disturbance $w = [w_1, \cdots, w_n]$ on all the agents to their position tracking errors $\tilde{p} = [\tilde{p}_1, \cdots, \tilde{p}_N]$ is given by

$$\begin{aligned} G_{\mathrm{ATA}}(s) = G(s) &= \left(s^2 I + (b_0 s + k_0) L\right)^{-1} = M(s^2 I + (b_0 s + k_0)\Lambda)^{-1} M^{\mathrm{T}} \\ &= M \begin{bmatrix} G_1(s) & & \\ & \ddots & \\ & & G_N(s) \end{bmatrix} M^{\mathrm{T}}, \end{aligned} \tag{A.32}$$

where $G_\ell(s)$ is given in (A.13) and M is the orthonormal matrix given as before. The H_∞ norm of $G_{\mathrm{ATA}}(s)$ (i.e., $A_{\mathrm{ATA}}^{\mathrm{linear}}$) is now given by

$$\begin{aligned} \|G_{\mathrm{ATA}}\|_{H_\infty} &= \sup_\omega \|G_{\mathrm{ATA}}(j\omega)\|_2 = \sup_\omega \sqrt{\lambda_{\max}(G_{\mathrm{ATA}}^*(j\omega) G_{\mathrm{ATA}}(j\omega))} \\ &= \sup_\omega \max_\ell \frac{1}{\sqrt{(-\omega^2 + \lambda_\ell k_0)^2 + b_0^2 \omega^2 \lambda_\ell^2}} = \max_\omega \max_\ell \|G_\ell(j\omega)\| = \max_\ell A_\ell = A_1, \end{aligned}$$

where A_1 is given in (A.14). Again, for large N, we obtain from (A.28) the following:

$$A_1 \geqslant \frac{1}{b_0 \sqrt{k_0}} \frac{(2N+1)^3}{\pi^3}. \tag{A.33}$$

In addition, using $\lambda_1 < 2k_0/b_0^2$ and $\frac{1}{\lambda_\ell^{3/2}} \leqslant \frac{(2N+1)^3}{8}$, we have

$$A_1 = \frac{2}{\lambda_1^{3/2} b_0 \sqrt{4k_0 - \lambda_1 b_0^2}} \leqslant \frac{2}{\lambda_1^{3/2} b_0 \sqrt{2k_0}} \leqslant \frac{(2N+1)^3}{4 b_0 \sqrt{2k_0}}. \tag{A.34}$$

Combining (A.33) and (A.34), we obtain

$$\left(\frac{1}{b_0 \sqrt{k_0} \pi^3} \right) (2N+1)^3 \leqslant A_{\mathrm{ATA}}^{\mathrm{linear}} \leqslant \left(\frac{1}{4 b_0 \sqrt{2k_0}} \right) (2N+1)^3, \quad \forall\, N.$$

Copyright © 2012 John Wiley & Sons, Ltd.

DOI: 10.1002/rnc

To have the asymptotic formula, when N is large, we use the approximation $\lambda_1 \approx \frac{\pi^2}{4N^2}$. Therefore, $\lambda_1 < 2k_0/b_0^2$ is true for large enough N irrespective of the values of k_0 and b_0. Substituting $\lambda_1 \approx \frac{\pi^2}{4N^2}$ into (A.14) and (A.15), we obtain that $A_1 \approx \frac{8N^3}{\sqrt{k_0}b_0\pi^3}$ and $\omega_{\rm p} = \omega_1 \approx \frac{\sqrt{k_0}\pi}{2N}$. Because $A_{\rm ATA}^{\rm linear} = A_1$, this concludes the proof.

□

Proof of Corollary 1

We first rewrite the coupled-ODE model (7) with linear controller as

$$\ddot{\tilde{p}} + b_0 L\dot{\tilde{p}} + k_0 L\tilde{p} = v_1 \sin(\omega_1 t), \tag{A.35}$$

where L is given in (A.9) and v_1 is the eigenvector of L corresponding to the smallest eigenvalue λ_1 given in (A.11). By the method of eigenfunction expansion [44], we can write $\tilde{p}(t) = \sum_{\ell=1}^{N} v_\ell h_\ell(t)$, where v_ℓ's are the eigenvectors of L given in (A.11). Substituting it into (A.35), we obtain

$$\sum_{\ell=1}^{N}\Big(v_\ell \ddot{h}_\ell(t) + b_0 L v_\ell \dot{h}_\ell(t) + k_0 L v_\ell h_\ell(t)\Big) = v_1 \sin(\omega_1 t).$$

Because of the superposition property of linear system, the aforementioned equation can be split into N ODEs by using $Lv_\ell = \lambda_\ell v_\ell$:

$$\ddot{h}_1(t) + b_0\lambda_\ell \dot{h}_1(t) + k_0\lambda_\ell h_1(t) = \sin(\omega_1 t),$$
$$\ddot{h}_\ell(t) + b_0\lambda_\ell \dot{h}_\ell(t) + k_0\lambda_\ell h_\ell(t) = 0, \quad \ell \in \{2, \cdots, N\}.$$

Following straightforward algebra, the steady-state response of each $h_\ell(t)$ is given by

$$h_1(t) = A_1 \sin(\omega_1 t + \psi_1), \qquad h_\ell(t) = 0, \quad \ell \in \{2, \cdots, N\},$$

where A_1 is given in (A.14). Thus, the steady-state response of $\tilde{p}$ is given by $\tilde{p} = v_1 A_1 \sin(\omega_1 t + \psi_1)$, which yields $\frac{\|\tilde{p}\|_{\mathcal{L}_2}}{\|w\|_{\mathcal{L}_2}} = A_1$. Recall from Theorem 5 that $A_{\rm ATA}^{\rm linear} = A_1$; we complete the proof. □

A 'proof' of the conjecture is as follows. First, notice that

$$A_{\rm FTL}^{\rm linear} = \sup_\omega |G_{\rm FTL}(j\omega)| \leqslant \sup_\omega |T(j\omega)| + \sup_\omega |Z(j\omega)| = |T(j\omega_1)| + \sup_\omega |Z(j\omega)|.$$

When N is large, the smallest eigenvalue $\lambda_1 \approx \frac{\pi^2}{4N^2}$ and $\sin\frac{N\pi}{2N+1} \approx 1$. The expression $|T(j\omega_1)|$ is then approximately given by

$$|T(j\omega_1)| \approx \frac{4}{2N+1}\frac{\pi}{2N+1}A_1 \approx \frac{4}{2N+1}\frac{\pi}{2N+1}\frac{(2N+1)^3}{b_0\sqrt{k_0}\pi^3} \approx \frac{8N}{\sqrt{k_0}b_0\pi^2}. \tag{A.36}$$

Under the assumption that N is large, the $O(N)$ term in the upper bound of $\sup_\omega |Z(j\omega)|$, which is given in (A.24), dominates the $O(1)$ term. Moreover, this $O(N)$ term is still smaller than $|T(j\omega_1)|$ given in (A.36). Notice that this upper bound is obtained by letting each term in $|Z(j\omega)|$ containing $G_\ell(j\omega)$ ($\ell \in \{1, 2, \cdots, N\}$) to achieve their maximum. In fact, the maximum of $|G_{\rm FTL}(j\omega)|$ can be only achieved at a single frequency. We thus conjecture that this frequency should be equal to ω_1, with the peak frequency corresponding to the principal model λ_1. This idea is similar to that a wave equation's resonance is achieved at the peak frequency and corresponds to its principle mode [44], and its H_∞ norm is determined by the peak response of the principle mode. Now, the H_∞ norm of $G_{\rm FTL}(s)$ is given by $\|G_{\rm FTL}(j\omega)\| = |G(j\omega_1)|$. Thus, from (A.17), we have

$$|T(j\omega_1)| - |Z(j\omega_1)| \leqslant \sup_\omega |G(j\omega)| \leqslant |T(j\omega_1)| + |Z(j\omega_1)|$$

When $N \gg 1$, the lower and upper bounds will be dominated by the term $|T(j\omega_1)|$, because $|Z(j\omega_1)|$ is $O(\ln(N-1))$ but $|T(j\omega_1)|$ is $O(N)$. Thus, the H_∞ norm of $G_{\rm FTL}(s)$ is determined by $|T(j\omega_1)|$. From (A.36), we have the firs-to-last amplification $A_{\rm FTL}^{\rm linear} \approx |T(j\omega_1)| = \frac{8N}{\sqrt{k_0}b_0\pi^2}$.

Copyright © 2012 John Wiley & Sons, Ltd.

DOI: 10.1002/rnc

ACKNOWLEDGEMENTS

This work was supported by the National Science Foundation through grants CNS-0931885 and ECCS-0925534.

REFERENCES

1. Hedrick JK, Tomizuka M, Varaiya P. Control issues in automated highway systems. *IEEE Control Systems Magazine* 1994; **14**:21–32. DOI: 10.1109/37.334412.
2. Ioannou P. *Automated Highway Systems*. Plenum Pub Corp: New York, 1997.
3. Tanner H, Christodoulakis D. Decentralized cooperative control of heterogeneous vehicle groups. *Robotics and Autonomous Systems* 2007; **55**(11):811–823.
4. Hoffman T. GRAIL: gravity mapping the moon. *IEEE Aerospace Conference*, Big Sky, MT, 2009; 1–8, DOI: 10.1109/AERO.2009.4839327.
5. Okubo A. Dynamical aspects of animal grouping: swarms, schools, flocks, and herds. *Advances in Biophysics* 1986; **22**:1–94.
6. Ioannou P, Chien C. Autonomous intelligent cruise control. *IEEE Transactions on Vehicular Technology* 1993; **42**(4):657–672.
7. Ioannou P, Xu Z, Eckert S, Clemons D, Sieja T. Intelligent cruise control: theory and experiment. *Decision and Control, 1993., Proceedings of the 32nd IEEE Conference on,* IEEE, San Antonio, TX, 1993; 1885–1890.
8. Bjornberg A. Autonomous intelligent cruise control. *Vehicular Technology Conference, 1994 IEEE 44th,* IEEE, Stockholm, Sweden, 1994; 429–433.
9. Darbha S, Rajagopal K. Intelligent cruise control systems and traffic flow stability. *Transportation Research Part C: Emerging Technologies* 1999; **7**(6):329–352.
10. Darbha S, Hedrick J. String stability of interconnected systems. *IEEE Transactions on Automatic Control* 1996; **41**(3):349–356.
11. Darbha S, Hedrick J, Chien C, Ioannou P. A comparison of spacing and headway control laws for automatically controlled vehicles. *Vehicle System Dynamics* 1994; **23**(8):597–625.
12. Zhang Y, Kosmatopoulos EB, Ioannou PA, Chien CC. Autonomous intelligent cruise control using front and back information for tight vehicle following maneuvers. *IEEE Transactions on Vehicular Technology* 1999; **48**:319–328.
13. Klinge S, Middleton R. Time headway requirements for string stability of homogeneous linear unidirectionally connected systems. *Proceedings of the 48th IEEE Conference on Decision and Control,* IEEE, Shanghai, China, 2009; 1992–1997.
14. Seiler P, Pant A, Hedrick JK. Disturbance propagation in vehicle strings. *IEEE Transactions on Automatic Control* 2004; **49**:1835–1841.
15. Lestas I, Vinnicombe G. Scalability in heterogeneous vehicle platoons. *American Control Conference*, New York, 2007; 4678–4683.
16. Liu X, Goldsmith A, Mahal S, Hedrick J. Effects of communication delay on string stability in vehicle platoons. *Intelligent Transportation Systems, 2001. Proceedings. 2001 IEEE,* IEEE, Oakland, CA, 2001; 625–630.
17. Peppard L. String stability of relative-motion PID vehicle control systems. *IEEE Transactions on Automatic Control* 1974; **19**(5):579–581.
18. Chu K. Decentralized control of high-speed vehicular strings. *Transportation Science* 1974; **8**(4):361.
19. Stotsky A, Chien C, Ioannou P. Robust platoon-stable controller design for autonomous intelligent vehicles. *Proceedings of the 33rd IEEE Conference on Decision and Control, vol. 3,* IEEE, Lake Buena Vista, FL, 1994; 2431–2436.
20. Bose A, Ioannou P. Environmental evaluation of intelligent cruise control (ICC) vehicles. *Intelligent Transportation Systems, 2000. Proceedings. 2000 IEEE,* IEEE, Dearborn, MI, 2000; 352–357.
21. Middleton R, Braslavsky J. String instability in classes of linear time invariant formation control with limited communication range. *IEEE Transactions on Automatic Control* 2010; **55**(7):1519–1530.
22. Khatir ME, Davison EJ. Decentralized control of a large platoon of vehicles using non-identical controllers. *Proceedings of the 2004 American Control Conference*, Boston, MA, 2004; 2769–2776.
23. Barooah P, Hespanha J. Error amplification and disturbance propagation in vehicle strings with decentralized linear control. *44th IEEE Conference on Decision and Control,* IEEE, Seville, Spain, 2005; 4964–4969.
24. Jovanović MR, Bamieh B. On the ill-posedness of certain vehicular platoon control problems. *IEEE Transactions Automatic Control* 2005; **50**(9):1307–1321.
25. Munz U, Papachristodoulou A, Allgower F. Robust consensus controller design for nonlinear relative degree two multi-agent systems with communication constraints. *IEEE Transactions on Automatic Control* 2011; **56**(1): 145–151.
26. Yadlapalli SK, Darbha S, Rajagopal KR. Information flow and its relation to stability of the motion of vehicles in a rigid formation. *IEEE Transactions on Automatic Control* 2006; **51**(8):1315–1319.
27. Darbha S, Pagilla PR. Limitations of employing undirected information flow graphs for the maintenance of rigid formations for heterogeneous vehicles. *International Journal of Engineering Science* 2010; **48**(11):1164–1178.
28. Veerman J. Stability of large flocks: an example July 2009. arXiv:1002.0768.

Copyright © 2012 John Wiley & Sons, Ltd.

29. Bamieh B, Jovanovic M, Mitra P, Patterson S. Coherence in large-scale networks: dimension dependent limitations of local feedback. *IEEE Transactions on Automatic Control* 2012. DOI: 10.1109/TAC.2012.2202052. (Available from: http://arxiv.org/abs/1112.4011v1) [Accessed date May 2012] in press.
30. Lin F, Fardad M, Jovanovic M. Optimal control of vehicular formations with nearest neighbor interactions. *IEEE Transactions on Automatic Control* 2012. DOI: 10.1109/TAC.2012.2181790. (Available from: http://arxiv.org/abs/1112.4113v1) [Accessed date December 2011] in press.
31. Stankovic S, Stanojevic M, Siljak D. Decentralized overlapping control of a platoon of vehicles. *IEEE Transactions on Control Systems Technology* 2000; **8**(5):816–832.
32. Jovanovic M, Fowler J, Bamieh B, D'Andrea R. On avoiding saturation in the control of vehicular platoons. *Proc. American Control Conference*, Boston, MA, 2004; **3**:2257–2262.
33. Warnick S, Rodriguez A. Longitudinal control of a platoon of vehicles with multiple saturating nonlinearities. *American Control Conference,* vol. 1, IEEE, Baltimore, MD, 1994; 403–407.
34. Khalil H. *Nonlinear Systems 3rd*. Prentice hall Englewood Cliffs: NJ, 2002.
35. Simon D. *Optimal State Estimation: Kalman, H [infinity] and Nonlinear Approaches*. John Wiley and Sons: Hoboken, NJ, 2006.
36. Bamieh B, Dahleh M. Exact computation of traces and H2 norms for a class of infinite-dimensional problems. *IEEE Transactions on Automatic Control* 2003; **48**(4):646–649.
37. Higham D. An algorithmic introduction to numerical simulation of stochastic differential equations. *SIAM Review* 2001; **43**(3):525–546.
38. Hao H, Barooah P. Decentralized control of large vehicular formations: stability margin and sensitivity to external disturbances. *Arxiv preprint arXiv:1108.1409* 2011, (Available from: http://arxiv.org/abs/1108.1409) [Accessed date August 2011]. DOI: 10.1109/TAC.2012.2191179.
39. Hao H, Barooah P. Control of large 1D networks of double integrator agents: role of heterogeneity and asymmetry on stability margin. *IEEE Conference on Decision and Control*, Atlanta, GA, 2010; 7395–7400. Expanded version: arXiv. 1011.0791.
40. Hao H, Barooah P, Mehta PG. Stability margin scaling of distributed formation control as a function of network structure. *IEEE Transactions on Automatic Control* 2011; **56**(4):923–929.
41. Hao H, Barooah P. On achieving size-independent stability margin of vehicular lattice formations with distributed control. *To appear in IEEE Transactions on Automatic Control* 2012. DOI: 10.1109/TAC.2012.2191179. Expanded version: arXiv: 1108.1844.
42. Hao H, Barooah P, Veerman J. Effect of network structure on the stability margin of large vehicle formation with distributed control. *Proceedings of the 49th IEEE Conference on Decision and Control*, Atlanta, GA, 2010; 4783–4788.
43. Yueh W, Cheng S. Explicit eigenvalues and inverses of tridiagonal Toeplitz matrices with four perturbed corners. *The Australian & New Zealand Industrial and Applied Mathematics (Anziam) Journal* 2008; **49**(3):361–388.
44. Haberman R. *Elementary Applied Partial Differential Equations: With Fourier Series and Boundary Value Problems*. Prentice-Hall: NJ, 2003.

Copyright © 2012 John Wiley & Sons, Ltd.